ACS Partner Journal
PRECISION CHEMISTRY
pubs.acs.org/PrecisionChem

Review

Molecular Interactions in Atomically Precise Metal Nanoclusters

Jing Qian, Zhucheng Yang, Jingkuan Lyu, Qiaofeng Yao,* and Jianping Xie*

Cite This: *Precis. Chem.* 2024, 2, 495−517

Read Online

ACCESS | Metrics & More | Article Recommendations

ABSTRACT: For nanochemistry, precise manipulation of nanoscale structures and the accompanying chemical properties at atomic precision is one of the greatest challenges today. The scientific community strives to develop and design customized nanomaterials, while molecular interactions often serve as key tools or probes for this atomically precise undertaking. In this Perspective, metal nanoclusters, especially gold nanoclusters, serve as a good platform for understanding such nanoscale interactions. These nanoclusters often have a core size of about 2 nm, a defined number of core metal atoms, and protecting ligands with known crystal structure. The atomically precise structure of metal nanoclusters allows us to discuss how the molecular interactions facilitate the systematic modification and functionalization of nanoclusters from their inner core, through the ligand shell, to the external assembly. Interestingly, the atomic packing structure of the nanocluster core can be affected by forces on the surface. After discussing the core structure, we examine various atomic-level strategies to enhance their photoluminescent quantum yield and improve nanoclusters' catalytic performance. Beyond the single cluster level, various attractive or repulsive molecular interactions have been employed to engineer the self-assembly behavior and thus packing morphology of metal nanoclusters. The methodological and fundamental insights systemized in this review should be useful for customizing the cluster structure and assembly patterns at the atomic level.

KEYWORDS: *gold, catalysis, conformational analysis, nanotechnology, noncovalent interactions, stereochemistry, luminescence*

1. INTRODUCTION

The investigation of material interactions represents a fundamental area of inquiry in the scientific community.[1−3] At the atomic level, a diverse array of intermolecular forces, including van der Waals forces and electrostatic interactions, has been extensively examined concerning their length scales and magnitudes. Drawing upon the comprehension of these intermolecular forces, various intriguing phenomena have been elucidated and diverse functional materials have been established. For instance, the deviation from ideal gas behavior can be partially attributed to the presence of intermolecular interactions. The capacity of capillary action to counteract gravity arises from the favorable intermolecular forces between the liquid and the wall. To give a more practical example, when scientists design a drug, ligand−receptor interaction should be considered for the efficacy of binding between drug molecules and the targeted sites and subsequent appropriate physiological response.

Having a core size of around 2 nm or below and possessing molecule-like properties, metal nanoclusters (NCs) serve as a bridge between organometallic compounds and plasmonic metal nanoparticles (>3 nm) and might be a good platform for studying molecular interactions.[4−7] Metal NCs possess a core−shell structure in which a metal core is protected by a layer of metal−ligand motifs. Furthermore, recent advances in crystallography reveal that metal NCs exhibit structure complexity comparable to that of natural proteins.[6,8] Additionally, because of their ultrasmall size, metal NCs display unique molecule-like properties that distinguish them from plasmonic nanoparticles. For instance, an atomically precise molecular formula can be used to describe NCs with a general form of $[M_n(L)_m]^q$, where n and m stand for the numbers of metal atoms (M) and ligands (L), respectively, while q is the net charge of an individual cluster. Furthermore, molecule-like properties are more prominent for NCs due to strong quantum confinement effects (when the de Broglie's wavelength of electrons is close to the dimension of the nanomaterials). Typical molecule-like properties arisen by this way include single electron transition between the highest occupied molecular orbital (HOMO) and the lowest unoccupied molecular orbital (LUMO),[9] intense photoluminescence,[10−13]

Received: May 25, 2024
Revised: July 30, 2024
Accepted: August 1, 2024
Published: August 23, 2024

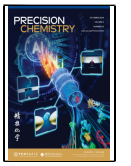

https://doi.org/10.1021/prechem.4c00044
Precis. Chem. 2024, 2, 495−517

intrinsic chirality,[14] inherent magnetism,[15,16] and marked catalytic selectivity and activity.[17,18] Due to the structure sensitivity of these molecule-like properties together with their atomically precise structure, metal NCs represent an ideal platform for studying the effects of molecular interactions on the structure and properties of metal nanomaterials at the molecular and atomic levels.

Systematic application of molecular interactions enables the precise modification and functionalization of metal NCs, spanning from their core to the ligand shell at the intracluster level, and extending to the assembly patterns at the intercluster level (as shown in Scheme 1). Despite having a layer of ligand protection, the very inner metal core structure can be affected and adjusted by molecular interactions. For the outer ligands, two contrasting strategies are often employed. The first strategy involves tightening the molecular structure and restricting the molecular motion, represented by an effort to increase the quantum yield of photoluminescence. Conversely, the second strategy creates space among the bundled-up ligands for access to small molecules, represented by the effort to improve the catalytic performance. However, it is worth noting that for both aspects, the interaction of NCs with surrounding molecules or the formation of assembly are also discovered to be important.[19] In the domain of self-assembly where NCs primarily interface with their counterparts,[1] the delicate balance between the size of nanomaterials and the interparticle interaction is a prerequisite for the formation of an ordered structure or even the rational design of crystal structure. Despite having some understanding of the inter- or intramolecular interactions, questions remain on the emergent phenomena, such as the conformational changes of NCs interacting with other molecules, similar to the induced-fit model for enzymes. Furthermore, with the atomically precise structure of NCs, directions, interaction sites, kinetics, or thermodynamics are possible parameters that can be studied for the nanoscale interactions. Hence, it is both important and feasible to delve deeper into learning about the nature of the molecular interaction of metal NCs at the nanoscale.

Scheme 1. Overview of Engineering Metal Nanoclusters from Metal Core Structure to the Ligand Shell (Which Encompasses Photoluminescence and Catalysis) and Finally to the Assembly Patterns via Molecular Interactions[a]

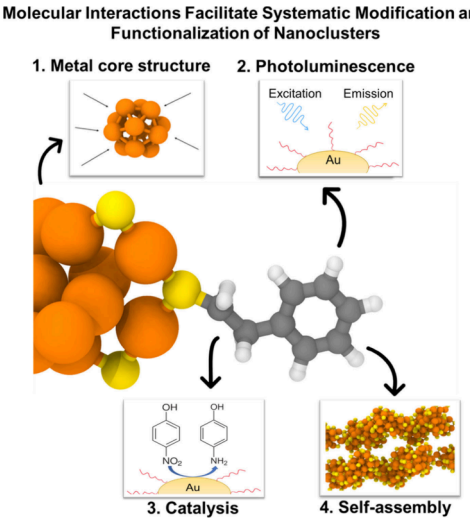

[a]Orange, Au; yellow, S; gray, C; white, H.

In this Perspective, we focus on the recent progress in the qualitative understanding of the molecular interaction of NCs, especially that of Au NCs. We demonstrate how these molecular interactions play a pivotal role in enabling the methodical modification and functionalization of NCs, encompassing their inner metal cores, the ligand layer, and the external assembly. Specifically, we discuss (1) surface interactions regulating metal core structure, (2) powering up photoluminescence, (3) tailoring catalytic performance, and (4) competing forces in self-assembly (as illustrated in Scheme 1). Through the discussion, questions, such as what the sites of interaction are or how the binding of small molecules changes the structure and properties of NCs, are highlighted. The deficiency in our current understanding is also pointed out. Finally, our perspectives on how to deepen our knowledge about the NCs' interaction in a more systematic or quantitative manner may be given. By highlighting the strategies to modify and functionalize our NCs, this review hopes that researchers can make more informed decisions and have more precise control over their nanomaterials.

2. SURFACE INTERACTIONS REGULATING METAL CORE STRUCTURE

Being the innermost core, the metal kernel, for instance, its packing mode, is one of the important structural features of NCs. Despite the ligand shell remaining the same, the properties of NCs can be drastically altered by a slight change in the positions or compositions of metal atoms. For instance, two isostructural NCs, $Au_{16}Cu_6(^t BuPhC{\equiv}C)_{18}$ and $Au_{22}(^t BuPhC{\equiv}C)_{18}$ were reported, where tBu refers to *tert*-butyl and Ph refers to phenyl, with the alloy counterpart having a near-unity photoluminescence quantum yield (PLQY). This much larger QY compared to that of Au_{22} might be attributed to the suppression of nonradiative decay by six doped copper in the metal core.[20] Hence, by fine-tuning the structure of metal core, researchers can achieve a precise control over NCs' properties. In this section, we advocate for one idea that surface forces can regulate the packing mode of the metal core. Under this idea, three themes can be brought together in unity, namely, the effects of ligands, solvents, and surfactants.

The intracluster ligand attraction or repulsion can affect the overall size or atom packing mode of metal core, of which ligand-exchange-induced size/structure transformation (LEIST) is a good example.[21−24] For instance, ligand-induced isomerization is reported by Chen et al.[25] As shown in Figure 1a, $Au_{28}(TBBT)_{20}$ (left structure), where TBBT stands for 4-*tert*-butylbenzenethiolate, subjected to heat and excess cyclohexanethiol treatment could transform into the structure shown on the right, where two trimeric staple-like SR-[Au-SR]$_3$ motifs (SR denotes a thiolate ligand) and two monomeric staple-like SR-Au-SR motifs surround the metal core that experiences a slight expansion. Similarly, $Au_{28}(SC_6H_{11})_{20}$, where SC_6H_{11} stands for cyclohexanethiolate, subjected to heat and excess 4-*tert*-butylbenzenethiol treatment can reversibly transform back to the structure shown on the left, where four dimeric staple-like SR-[Au-SR]$_2$ motifs exist and the gold−gold distance in the metal core is shorter. Dispersion-corrected density functional theory (DFT) calculations revealed that the favorable van der Waals forces among the packing of ligands helped to stabilize the structure of $Au_{28}(TBBT)_{20}$. Additionally, the two NCs exhibit different

https://doi.org/10.1021/prechem.4c00044
Precis. Chem. 2024, 2, 495−517

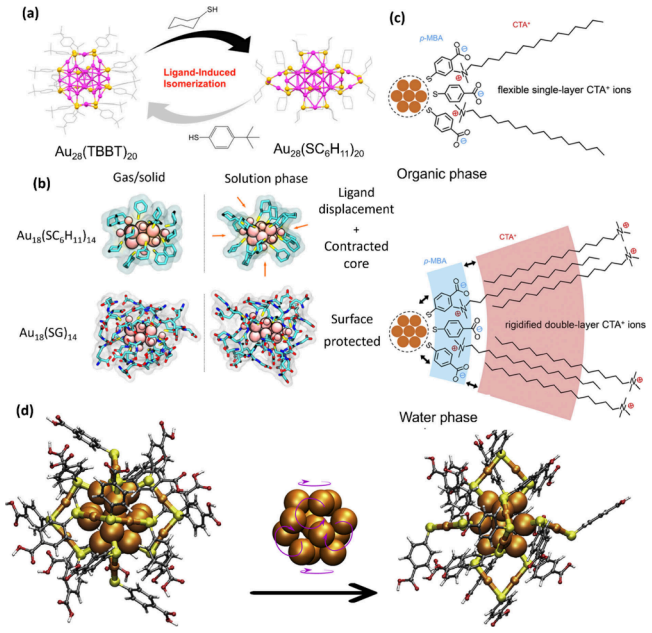

Figure 1. (a) Ligand-induced isomerization between $Au_{28}(TBBT)_{20}$ and $Au_{28}(SC_6H_{11})_{20}$. Pink, Au; yellow, S; gray sticks, ligands. Reprinted with permission from ref 25. Copyright (2016) American Chemical Society. (b) Structures of $Au_{18}(SC_6H_{11})_{14}$ and $Au_{18}(SG)_{14}$ in solution or solid phase. Pink balls, Au; yellow sticks, S; cyan sticks, C; red sticks, O; blue sticks, N. Reprinted with permission from ref 26. Copyright (2018) American Chemical Society. (c) Schematic illustration of CTA^+ ions adsorbed onto the $[Au_{25}(p\text{-MBA})_{18}]^-$ NCs through intermolecular interaction in both oil and water phases. (d) Structures of the two $[Au_{25}(p\text{-MBA})_{18}]^-$ NC isomers and the conversion process between two isomers. Large orange spheres, core Au_{13} atoms; small orange spheres, ligand Au atoms; yellow, S; gray, C; red, O; white, H. Panels c and d are reprinted with permission from ref 30. Copyright (2021) Elsevier Inc.

catalytic performances in the CO oxidation reaction after being deposited onto a CeO_2 support.

The effect of solvents on the metal core structure is more subtle. A series of extended X-ray absorption fine structure (EXAFS) studies were carried out to reveal the change in distances between atoms.[26−28] For $Au_{18}(SR)_{14}$, the interaction between ligands and the solvent environment plays a crucial role in determining the morphology of NCs. Two ligands, cyclohexanethiolate (SC_6H_{11}) and glutathione (SG), were compared by Chevrier et al.[26] For cyclohexanethiolate, when the solid-phase NC was dissolved in toluene, toluene interacted with ligands through the CH···π interaction. The ligand shell was thus disturbed, and the metal core contracted (Figure 1b), opening more room for the access of small molecules. In contrast, glutathione formed strong intraligand hydrogen bonding. As a result, the Au−Au bonding distance in the metal core remains almost the same in the solid or aqueous phase. In another work concerning $Na_4Ag_{44}(p\text{-MBA})_{30}$ (*p*-MBA denotes 4-mercaptobenzoic acid),[27] aprotic solvents favored the interaction with silver and caused the shortening of the silver distance in the core, while water clouded around *p*-MBA ligands and merely affected the structure of Ag core. Under semiaqueous conditions, a shell of steric protection was provided by the solvent molecules, providing extra stability to the NC and potentially affecting catalytic or biomedical properties. Therefore, distances between atoms in the metal core can also be adjusted by the interplay between ligands and the NC's solvent environment.

Also, the effect of intermolecular interactions can be induced by the surfactants on the atom packing mode of the metal cluster core. In 2020, Matus et al. theoretically predicted two topological isomers of $Au_{25}(SR)_{18}$, whose structure differed by the rotation of the Au_{13} core.[29] The energy barrier of this rotation or theoretical isomerization is small. Thus, such isomerization was realized experimentally by Cao et al. via the addition of surfactants.[30] 12 CTA^+ ions (CTA^+ denotes cetyltrimethylammonium) as the first adsorbed layer (Figure 1c) had the CH···π interaction with the benzene groups of $[Au_{25}(p\text{-MBA})_{18}]^-$ NCs, triggering the isomerization as seen in Figure 1d. The isomerization also induced changes in optical properties, with the solution color changing from reddish brown to dark green. In summary, surface forces could have a significant effect on the atomic structure of NCs. By understanding the rules behind intermolecular interactions, we can fine-tune the structures of the nanomaterials.

3. POWERING UP PHOTOLUMINESCENCE

Tremendous efforts have been devoted to improving the photoluminescence quantum yield (PLQY) of the NCs. The ligand shell represents the primary site where various engineering strategies involving molecular interactions are employed to enhance the photoluminescence of NCs. Given the strong quantum-size effect, the emission of Au NCs is strongly size- and composition-dependent. Therefore, "molecular surgery" strategies like heteroatom doping[20,31,32] and removing/adding core metal atom[33] have been developed to power up the photoluminescence. However, controlling the composition and geometry of NCs is a complex and challenging task. As suggested by recent contributions by Jin and co-workers, boosting PLQY through alloying metal NCs requires precise control over the location and number of heteroatoms.[34]

To avoid the challenging and tricky synthesis task, alternative approaches such as the restriction of intramolecular motion (RIM) including both vibration and rotation may be considered as efficient options for enhanced emission. Common RIM strategies include aggregation, surface rigidification, and spatial confinement, which can be made possible by diverse interactions of $\pi-\pi$ stacking, hydrogen bonding, van der Waals forces, and ionic pairing. Thus, the interactions between the ligands of metal NCs and small molecules to enhance cluster photoluminescence are discussed in this section. The discussion is divided into three subsections corresponding to cluster structure modification at the intracluster level, intercluster level, and cluster interactions with adsorbed small molecules.

3.1. Surface Engineering toward Enhanced Photoemission

In pursuit of highly luminescent metal NCs, significant progress has been made since Xie and co-workers first extended the scope of aggregation-induced emission (AIE) from molecular chemistry into inorganic nanochemistry in 2012.[35,36] While the Au(0) core plays a role in AIE, surface engineering stands as the primary method of enhanced emission. Many research efforts have focused on investigating the interface between surface ligands and external molecules to achieve RIM. For thiolate ligands, the introduction of bulky counterions has become a rather good option. Lee and co-workers employed tetraoctylammonium (TOA) cations to

https://doi.org/10.1021/prechem.4c00044
Precis. Chem. 2024, 2, 495−517

electrostatically bond with the negatively charged $Au_{22}(SG)_{18}$ clusters. The resultant TOA-Au_{22} clusters exhibited UV−vis spectra similar to those of pristine Au_{22} NCs, but up to ∼62% PLQY due to the surface rigidification achieved by ionic pairing. Interestingly, a less bulky counterion (CTA^+) failed to enhance the cluster emission.[19] To further improve RIM, a recent study integrated hydrogen bonds as another key attribute to rigidify the surface. The introduction of L-arginine (ARG) to the ligand shell of 6-aza-2-thiothymine (ATT)-protected Au NCs led to a significant increase in PLQY from 1.8% to 65%.[37] The surface rigidification was achieved through multiple hydrogen bonds between the guanidine group of ARG and ATT, which drastically increased the PLQY. Recently, a layer-by-layer engineering strategy was developed (Figure 2a), in which ATT was bonded to the gold surface with covalent bonds (ATT-protected Au_{10} NCs), followed by hydrogen bonds between ATT and ARG.[38] TOA served as the third shell, which electrostatically interacted with the carboxyl anions of ATT (Figure 2b and 2c). This resulted in a greatly improved surface rigidity of Au NCs, with a high PLQY of 90.3 ± 3.5%. The electronic properties and local structures remained unchanged, as confirmed by Au L3 edge X-ray absorption near-edge structure (XANES) and extended Fourier-transformation X-ray adsorption fine structure spectra (FT-EXAFS). Known from the identical optical spectra of Au NCs before and after surface rigidification, these noncovalent interactions have little influence on the electronic states but rather activated RIM and changed the relaxation pathway, thereby enhancing the emission of NCs.

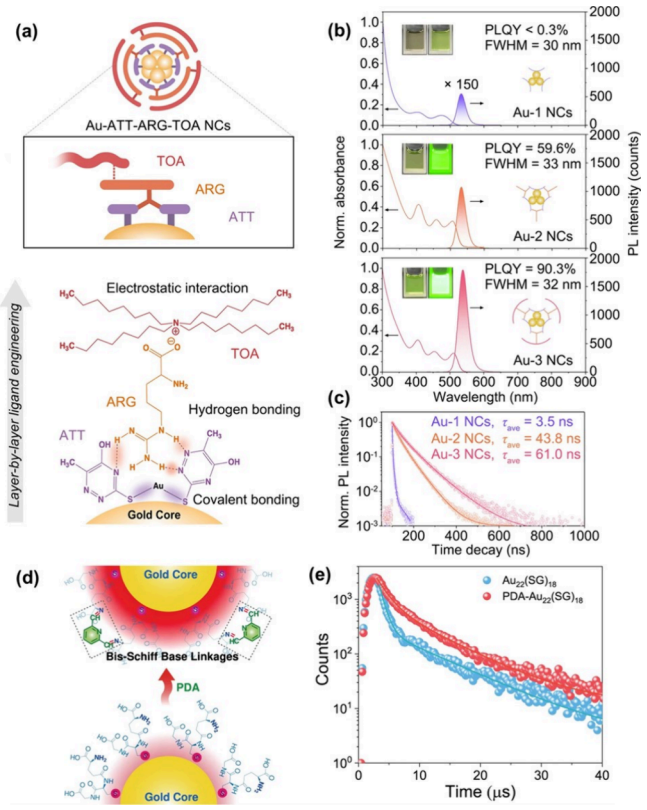

Figure 2. (a) Schematic illustration of the triple-ligand layer-by-layer self-assembly approach for luminescent enhancement of Au NCs. The schematic items colored in purple, orange, and pink denote Au NCs coated with ATT, ARG, and TOA ligands, respectively. (b) UV−vis absorption and luminescence spectra of Au-1 (ATT-Au), Au-2 (ATT-ARG-Au), and Au-3 (ATT-ARG-TOA-Au) NCs; the insets are the digital optical photographs of Au-1, Au-2, and Au-3 NCs under ambient atmosphere (left) and 365 nm light irradiation (right). The corresponding prototypes of each NC are depicted in individual spectrum. (c) Luminescence time-resolved spectra of Au-1, Au-2, and Au-3 NCs upon 405 nm excitation. Panels a−c are reprinted with permission from ref 38. Copyright (2023) Springer Nature. (d) Schematic of how emission intensity is enhanced through the binding of PDA. The red shadings represent PL intensities of $Au_{22}(SG)_{18}$ NCs before and after the addition of PDA. (e) Comparison of the luminescence decay of $Au_{22}(SG)_{18}$ NCs and $Au_{22}(SG)_{18}$ NCs after the binding of PDA. Panels d and e are reprinted with permission from ref 44. Copyright (2022) Springer Nature.

Another prominent category of AIE strategies involves the utilization of polymers. The macromolecules used are often biocompatible, rendering them suitable for various biomedical applications.[39−43] Moreover, polymers serving as carriers can potentially enhance the colloidal stability of NCs, further expanding their utility in biological systems. A notable example is chitosan, a common biomedical cationic polymer, which has been employed to form hydrogels with AuNCs, resulting in a 3-fold enhancement in PLQY.[43] This enhancement is hypothesized to stem from strong electrostatic interaction between the amine groups of chitosan and carboxylate groups of the NCs' ligand, which may contribute to RIM. Interestingly, the PL emission wavelength of the hydrogel can be modulated from green to orange and deep red by adjusting the ratio of gold to thiolates. However, it is important to note that in many applications involving polymer-induced PL enhancement, the complex chemical environment with multiple species presents a significant challenge to further detailed investigation.

Although the concept of covalent bonding falls beyond the scope of supramolecular interaction, this review still wants to mention a few papers in which covalent bonds are also applied to construct a rigidified surface for RIM. Of note, covalent bonds can also serve as a contributing factor in combination with various noncovalent interactions to achieve the luminescence improvement. The functional groups carried by surface ligands, such as amine groups, can be designed as active sites for covalent modifications. Chen and co-workers utilized a simple chemical reaction to build bis-Schiff base linkages between PDA (2,6-pyridinedicarboxaldehyde) and the surface amine groups of $Au_{22}(SG)_{18}$ through imine bonds (Figure 2d and 2e).[44] The covalent bonds are expected to be more stable and therefore have a stronger influence on RIM. The interactions between PDA and $Au_{22}(SG)_{18}$ were carefully examined, where a typical imine stretching vibration was clearly displayed in the FT-IR (Fourier-transform infrared spectroscopy) spectrum. Furthermore, PDA-$Au_{22}(SG)_{18}$ exhibited enhanced emission with a PLQY of up to 48% and a faster relaxation process, which can be attributed to the promoted core−shell transition resulting from a reduction in the interaction distance between the core and the shell upon the formation of bis-Schiff base bonds. More surface engineering strategies with covalent bonds to the ligands of NCs were reported, such as those involving conjugation with benzyl chloroformate (CBz-Cl).[45,46] Interestingly, while the conjugation involves small aromatic molecules, the enhancement of emission cannot be solely attributed to the covalent bonds. This is because both PDA and CBz-Cl are aromatic and could have abundant intermolecular $\pi-\pi$ interactions, and thus, it is important to consider the joint effect of these forces.

https://doi.org/10.1021/prechem.4c00044
Precis. Chem. 2024, 2, 495−517

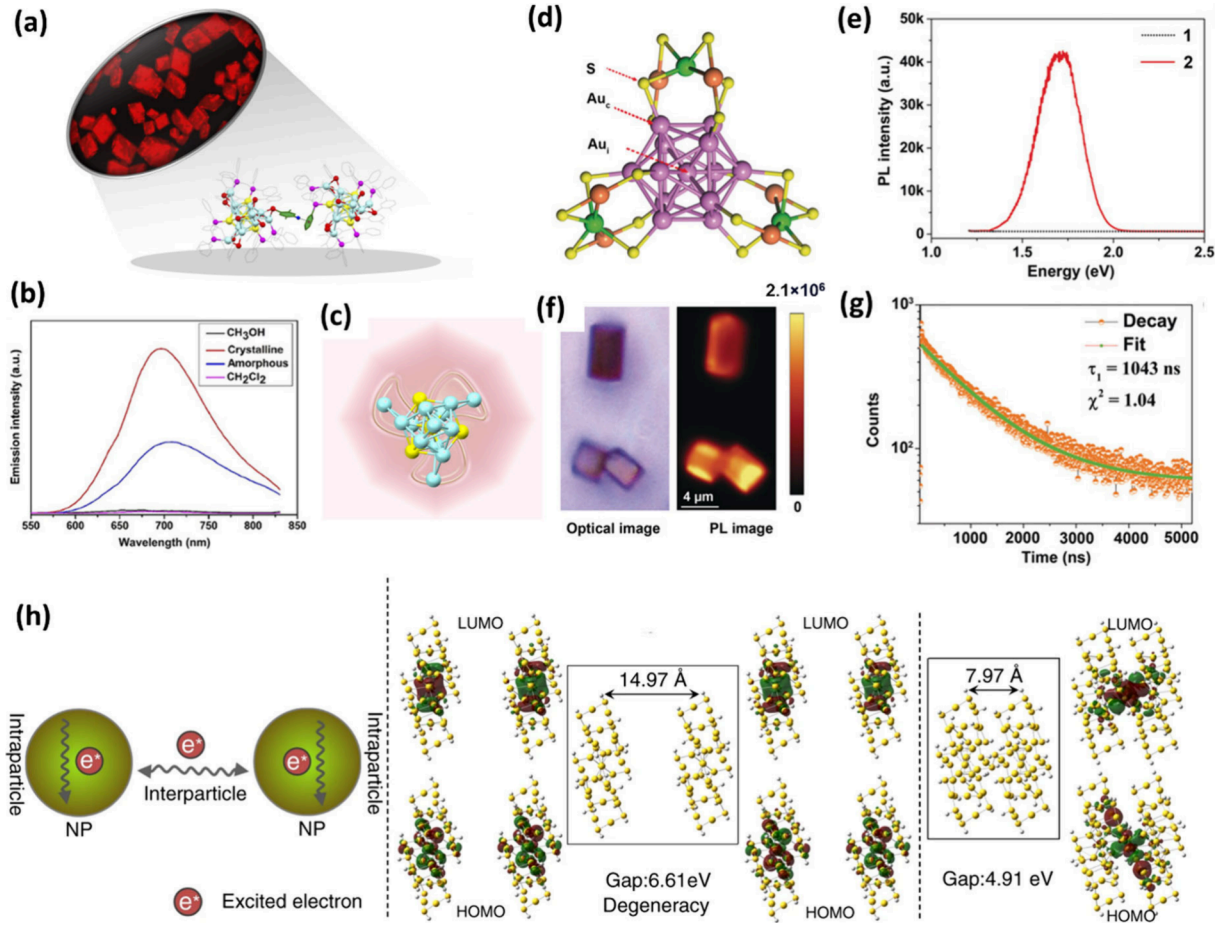

Figure 3. (a) Fluorescent optical microscopy of $Au_4Ag_{13}(DPPM)_3(SR)_9$ NCs shown in the upper left and CH···π interactions between two NCs shown in the bottom. Light blue, Ag; yellow, Au; magenta, P; red, S; gray, C. (b) Emission spectra of the $Au_4Ag_{13}(DPPM)_3(SR)_9$ NCs in different states. Crystalline state is represented by the red line, CH_2Cl_2 solution phase by the magenta line, methanol solution phase by the black line, and amorphous states by the blue line. Excitation wavelength is at 500 nm. a.u. stands for arbitrary units. (c) Illustrative diagram for the triblade fan configuration to show the possibility of restricted intramolecular rotation. Light blue, Ag; yellow, Au. Panels a–c are reprinted with permission from ref 55. Copyright (2017) American Association for the Advancement of Science. (d) Core structure of 2 ($[Au_{19}Cd_3(SR^2)_{18}]^-$) NC. Purple/magenta, Au; yellow, S; green, Cd. (e) PL emission spectra of 1 ($[Au_{25}(SR^1)_{18}]^-$ cluster) and 2 ($[Au_{19}Cd_3(SR^2)_{18}]^-$) crystals. SR^1 stands for 2-phenylethanethiol and SR^2 stands for p-toluenethiol. (f) PL image of 2 ($[Au_{19}Cd_3(SR^2)_{18}]^-$) crystals. (g) PL decay curve of 2 ($[Au_{19}Cd_3(SR^2)_{18}]^-$) crystals. Panels d–g are reprinted with permission from ref 56. Copyright (2020) Wiley. (h) On the left, the scheme shows the interparticle and intraparticle nonradiative transfer of excited electrons. On the right, the HOMO–LUMO distributions and gaps are shown when the interparticle distances are 14.97 and 7.97 Å, respectively. Reprinted with permission from ref 31. Copyright (2020) Springer Nature.

It is worth noting that the intensity of the emission is closely associated with light absorption, highlighting the potential of conjugating surface ligands with light-harvesting molecules through covalent bonds. Energy is expected to be efficiently transferred from the donor to the metallic core through these covalent bridges. Herein, the functional groups with delocalized π-electrons and proper bandgap could be of paramount importance in designing highly luminescent NCs. In the previously mentioned reports, after covalently modified with CBz, Lee and co-workers further employed pyrene and folic acid to functionalize $Au_{22}(SG)_{18}$.[45,46] While pyrene served as a chromophore and a 5-fold PLQY enhancement was achieved, folic acid was used to sensitize the Au_{22} cluster by fluorescence resonance energy transfer (FRET). More studies have been reported based on the conjugation between Au NCs with lactoferrin, porphyrin, graphene, and azobenzene derivatives.[47,48]

3.2. Shining Strategies beyond the Single-Cluster Level

While small molecules could brighten NCs at the single-cluster level, supramolecular interaction at the intercluster level represents an alternative means for achieving emission enhancement. It has now become known that enhanced luminescence intensity, chirality, and many other collective properties can be induced, by arranging metal NCs into long-range-ordered superstructures based on noncovalent interactions between NCs.[49−51] Similar to the conceptual innovation of AIE, crystallization-induced emission enhancement was also first demonstrated with organic compounds by Tang and co-workers in 2009.[52] Now, it is commonly accepted that in the highly ordered assembly of weak/nonemissive NCs, the compact structure deriving from the restricted movement of ligands and strengthened metallophilic interactions would improve the radiative energy relaxation channel via ligand-to-metal charge transfer (LMCT) and/or ligand-to-metal−metal charge transfer (LMMCT) processes.[49] Especially for the latter electronic transition, LMMCT, closer distances between

https://doi.org/10.1021/prechem.4c00044
Precis. Chem. 2024, 2, 495−517

metals in NCs or the assembly play a significant role in the PL properties of materials. Strategies following the notion of "unity is strength" have thus emerged to engineer the supramolecular forces toward solid-state strong emission, which is key to light-emitting device fabrication and many other applications.[53] It is worth noting that not all NCs can easily be grown into high-quality crystal. This is especially true for water-soluble metal NCs due to the diverse supramolecular interactions and the active surface dynamics of these NCs.[38,54] Therefore, self-assembly of metal NCs into less ordered superstructures by similar intercluster interactions is deemed an alternative approach to achieve emission enhancement beyond the single-cluster level.

Rational control and balance of the supramolecular forces of metal NCs are vital to crystallization induced emission enhancement. Zhu and co-workers reported crystallization induced emission enhancement phenomenon of atomically precise metal NCs in 2017 (Figure 3a).[55] In the case of the as-synthesized $Au_4Ag_{13}(DPPM)_3(SR)_9$ (DPPM denotes bis-(diphenylphosphino)methane), the NC was weakly emissive in solution but had strong emission at 695 nm in the crystalline state as shown in the emission spectra of Figure 3c. The structure of the NC was meticulously analyzed both experimentally and computationally to understand the reasons behind the emission enhancement. Although the single NC adopting a triblade configuration may experience RIM (Figure 3b), intermolecular interactions were used to explain the emission enhancement in the crystalline state. The close distances (~2.568 Å) between the hydrogen atoms of the thiolate ligand and the phenyl ring in DPPM led to strong C−H···π interactions. The absence of such interactions resulted in weaker luminescence in the amorphous state, where fewer C−H···π interactions were expected. The authors proposed a general strategy for brightening weakly/nonemissive NCs by rationally controlling the chemical environment and weak interactions. The surface restructuring of $[Au_{25}(SR^1)_{18}]^-$ with additional doping resulted in the formation of a new bimetallic $[Au_{19}Cd_3(SR^2)_{18}]^-$ as shown in Figure 3d (SR^1 stands for 2-phenylethanethiol and SR^2 stands for *p*-toluenethiol), which was characterized by single-crystal X-ray diffraction (SCXRD) and was found to have a denser packing in crystal compared with its precursor.[56] As a consequence of the compact packing, $[Au_{19}Cd_3(SR^2)_{18}]^-$ was surrounded by intracluster C−H···π and intercluster π···π interactions, leading to an increased emission intensity in their close-packed state (Figure 3e and 3f) and an altered electron relaxation pathway (Figure 3g).

Moreover, intermolecular hydrogen bonds and electrostatic interactions were also employed to boost luminescence for Au_8 NCs, which exhibited strong near-infrared (NIR) emission in the crystalline state.[57] While it is intuitively correct that denser structure will lead to stronger emission, a recent study by Gan et al. revealed that shortening interparticle distance could decrease photoluminescence.[31] In the crystal of $Au_{60}S_8(SCH_2Ph)_{36}$ under high pressure (SCH_2Ph stands for phenylmethanethiolate), shorter intercluster distance gave rise to stronger π···π stacking interactions, which lead to the overlapping of electron clouds and decreased the HOMO−LUMO gap of NCs (Figure 3h). Consequently, the non-radiative relaxation of excited electrons was accelerated, leading to the quenching of photoluminescence. This assertion is also supported by theoretical calculations. These seemingly contradictory observations underscore the significance of carefully balancing supramolecular forces and rationally designing intercluster distances toward achieving enhanced emission. Another popular choice of building blocks for assembly and PL enhancement is $(NH_4)_9[Ag_9(o\text{-MBA})_9]$, where *o*-MBA refers to 2-mercaptobenzoic acid or thiosalicylic acid.[58−60] Rich carboxylate groups on the ligands of this Ag NC allow for multiple intermolecular hydrogen bonding. With the addition of alcohol for antisolvent gelation or tartaric acid for cocrystallization,[59,60] PL intensity of AgNCs is enhanced, accompanied with a few intriguing optical property changes including fluorescence-to-phosphorescence switching or chiral transfer.

Metallophilic interactions, which are attractive interactions between d^8 and d^{10} transition metal ions (e.g., Pt(II), Au(I), Ag(I), and Cu(I)), can be utilized for enhancing the emissions of metal NCs. In a typical metallophilic scheme, the metal−metal distances are usually shorter than the sum of their van der Waals radius, rendering metallophilic interactions with similar bond strength to that of hydrogen bonds.[61] Inspired by aurophilic interactions-assisted assembly of luminescent gold-(I) complexes,[62,63] Wu et al. employed effective intercluster aurophilic interactions to assemble $[Au_{25}(p\text{-MBA})_{18}]^-$ NCs into ordered 1D nanobelts for enhanced emission (Figure 4a and 4b). By this way, the PLQY of pristine $[Au_{25}(SR)_{18}]^-$ NCs which is 10^{-4} originally can be significantly promoted up to 6.2%.[51] FT-EXAFS was employed to study the assembly behavior of $[Au_{25}(p\text{-MBA})_{18}]^-$, which revealed a shrinking metal core and stronger diffuse peaks of Au(I)···Au(I) interactions (Figure 4c). Therefore, it is reasonable to assign aurophilic interactions as the driving force to assemble Au NCs into 1D nanowires. Further assembly of the nanowires into emissive nanoribbons was predominantly directed by inter-ligand interactions, such as π−π stacking and dispersive interactions, along the longitudinal axis. This self-assembly evolution was supported by the presence of two distinct emission bands with different temperature responses. It is worth noting that metallophilic interactions play an important role in the self-assembly of chiral NCs and the regulation of circularly polarized photoluminescence (CPL) emission. For example, chiral Au_3 NCs with strong circular dichroism (CD) but free of CPL were synthesized and assembled into uniform body-centered cubic (BCC) packing nanocubes with a remarkable CPL response.[50] The emerging CPL response was attributed to the strong intermolecular CH···π interactions, which restrict rotation of the chiral ligands. Though the self-assembly process was not clearly depicted, aurophilicity has been clearly evidenced within the assembled nanocubes by a measured Au−Au bond length of ~2.676 Å that falls well into the regime of aurophilic interactions. Intercluster aurophilicity was also used to string chiral Au_4 clusters together, resulting in a much higher PLQY of 41.4% and an intense CPL response simultaneously compared to their nonemissive monomers.[64] Overall, metallophilic interactions are often combined with versatile noncovalent forces to build assembled structures with exceptional properties.

3.3. Molecule Adsorption Matters: Quench or Enhance?

The impact of molecular oxygen adsorption on the emission properties of NCs has been extensively studied. In general, molecular oxygen (O_2) is known to quench phosphorescence, while fluorescence remains unaffected. The quenching process is known as "collisional quenching", where the excited triplet state molecule interacts with two unpaired electrons of parallel spins in its ground state, thereby accepting the energy

https://doi.org/10.1021/prechem.4c00044
Precis. Chem. 2024, 2, 495−517

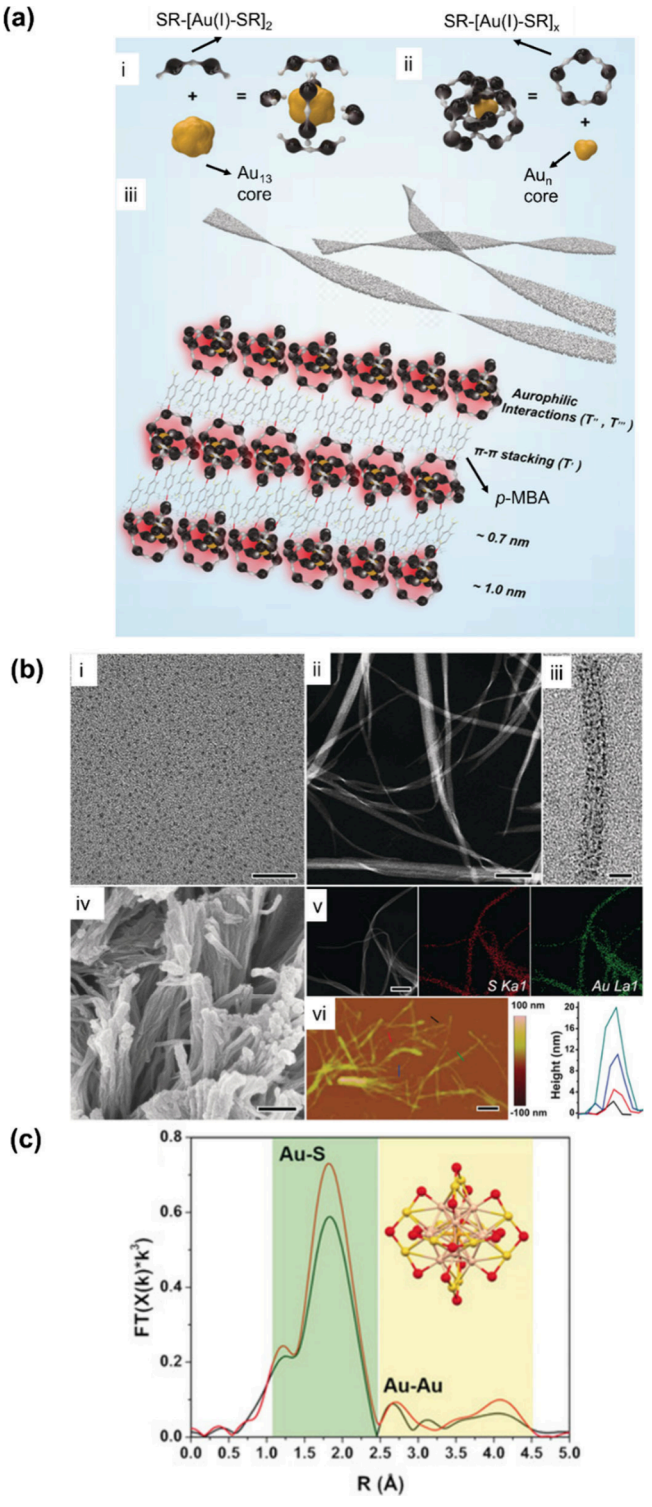

Figure 4. (a) Schematic demonstration of self-assembly from isolated $[Au_{25}(SR)_{18}]^-$ NCs into nanoribbons. The cartoons illustrate (i) the original structure of $[Au_{25}(SR)_{18}]^-$ NCs and (ii) the smaller NCs formed from self-assembly, as well as (iii) spatial arrangement of NCs in nanoribbons. (b) (i) TEM (transmission electron microscopy) image of $[Au_{25}(p\text{-MBA})_{18}]^-$ NCs. (ii–vi) High-angle dark-field scanning TEM (HAADF-STEM), high-resolution TEM (HR-TEM), scanning electron microscopy (SEM) images of the self-assembled nanoribbons of $[Au_{25}(p\text{-MBA})_{18}]^-$, HAADF-STEM image (left), corresponding energy-dispersive X-ray (EDX) element maps (middle and right), and atomic force microscopy (AFM) image of the nanoribbons. The scale bars are 20 nm (i), 300 nm (ii), 10 nm (iii), 300 nm (iv), 300 nm (v), and 300 nm (vi), respectively. (c) Au L3-edge FT-EXAFS spectrum of $[Au_{25}(p\text{-MBA})_{18}]^-$ NCs (black line) and the assembled nanoribbons (red line). Insert: the atomic structure of $[Au_{25}(p\text{-MBA})_{18}]^-$ (red, S; yellow/pink/orange, Au; *p*-MBA ligands except S are omitted for clarity). Panels a–c are reprinted with permission from ref 51. Copyright (2019) Wiley.

transferred from the molecule and causing it back to the ground state without emitting. This process competes with the radiative decay pathway, resulting in quenched phosphorescence.[65,66] Therefore, changes in emission intensity and lifetime under ambient conditions become a golden criterion to determine the intrinsic emission mechanism.[56,67−69] For instance, Zhu et al. designed careful control experiments over phosphorescent Pt_1Ag_{16} NCs and fluorescent Au_5Ag_{11} NCs.[67] The cycles between the emission enhanced with N_2 and quenched with the O_2 of Pt_1Ag_{16} readily indicated that the emission is phosphorescence in nature. Moreover, singlet $^1O_2$, the "product" of quenching, was detected in the emission spectra, unambiguously identifying the emission nature (Figure 5a, 5b, and 5c). A sensitive O_2 sensor switch (Ag_{12}(bpy)NC-based metal−organic frameworks, bpy denotes 4,4′-bipyridine) was developed following this mechanism.[70] The exceptional real-time quenching response was attributed to the highly O_2 permeable channels, weak interactions, and moderate phosphorescence lifetime. Computational work supported the sites of guests (O_2) in the cavity of Ag_{12}(bpy) NCs and proposed that O_2 readily interacted with the exposed bpy linker to transfer energy (Figure 5d and 5e). Of note, though being employed as testing molecules for emission nature and sensor development, O_2 is supposed to be avoided in most scenarios, especially for those with phosphorescent emission from the aggregation of Au NCs.[71,72]

In contrast, gas adsorption, including O_2, nitrogen, or argon, sometimes may not be a negative factor toward enhanced emission. In a self-assembled gold sulfido NC, a drop in emission intensity and PLQY was observed in a vacuum, providing strong evidence to argue against phosphorescence quenched by O_2.[73] The authors attributed this unexpected observation to the structural transformation of the unique quartet structure in this NC. Specifically, the removal of the gas led to a compaction of the interquartet void under vacuum (the gas could be air, argon, or pentane), which resulted in a more compacted crystal with an expanded central gold quartet (Figure 5f). This expansion leads to distortions and vibrations of the overall structure, resulting in a lower PLQY. Interestingly, the emission switching during the pump-fill cycle renders the gold quartet a promising responsive luminescent material. This observation highlights the limited understanding of the effects of gas adsorption on NCs, and the dynamic structure designs could offer new regulation methods over these effects. The interplay between the diverse adsorbents of Au NCs, including gas molecules, solvents, and solvated ions, and the emission property remains an open question. Therefore, further investigation is necessary to fully comprehend the underlying principles of gas adsorption on the emission properties of Au NCs.

4. TAILORING CATALYTIC PERFORMANCE

Interactions at the nanoscale are the foundation of any catalysis phenomenon. In heterogeneous catalysis, the crucial step of

https://doi.org/10.1021/prechem.4c00044
Precis. Chem. 2024, 2, 495−517

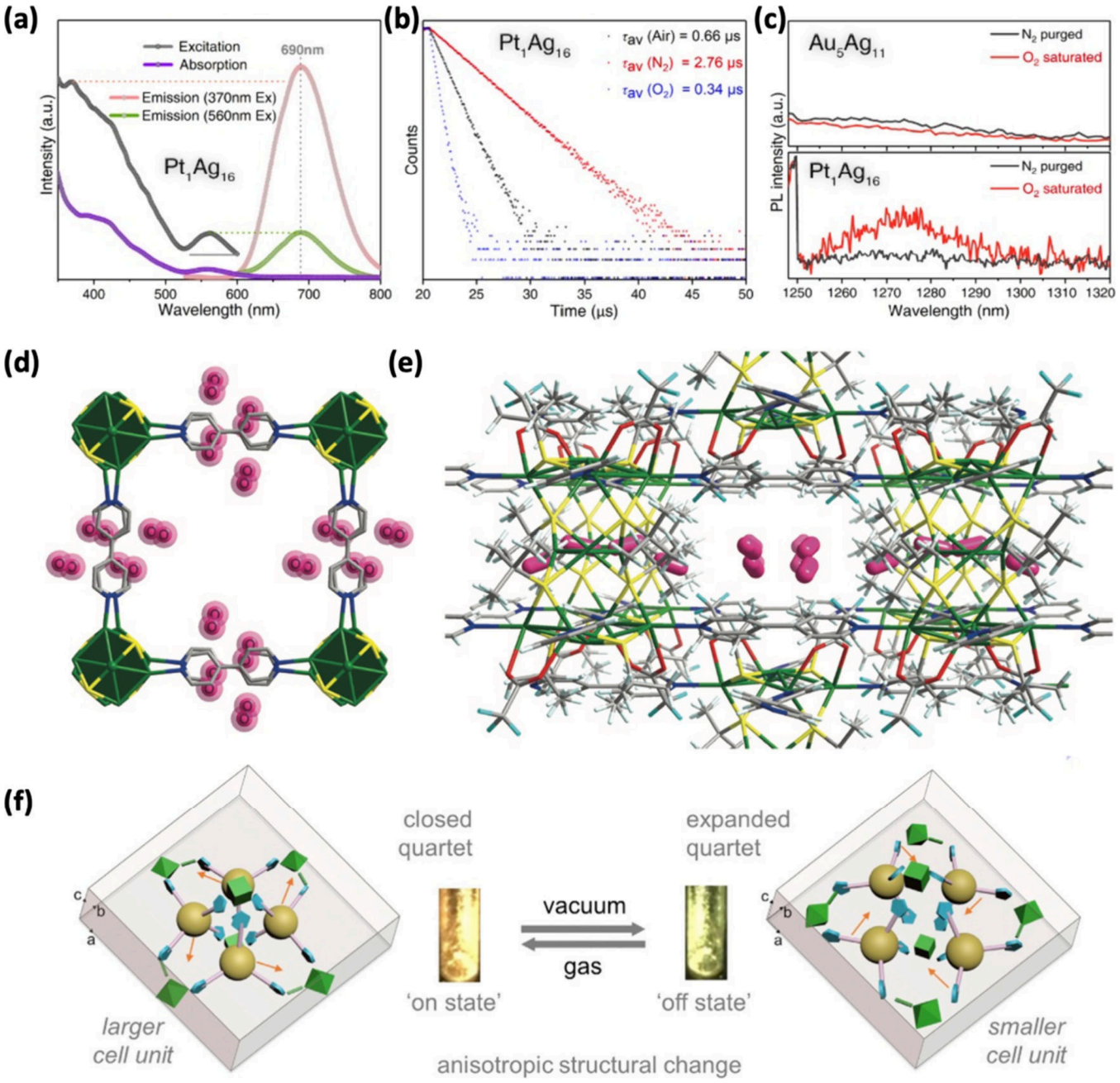

Figure 5. (a) Absorption (purple line), excitation (gray line), and emissions (pale red excited at 370 nm, pale green excited at 560 nm) of Pt_1Ag_{16} NCs in deaerated dichloromethane. (b) PL decay curves of Pt_1Ag_{16} NCs at room temperature under ambient (black dots), N_2-purged (red dots), and O_2-saturated (blue dots) conditions. (c) Near-infrared PL of N_2-purged (black line) and an O_2-saturated (red line) dichloromethane solution of Au_5Ag_{11} and Pt_1Ag_{16} NCs; excitation wavelength at 560 nm. Panels a–c are reprinted with permission from ref 67. Copyright (2022) Wiley. (d, e) Different views of Ag_{12}(bpy)-O_2 structure and locations of guest molecules in the cavity of Ag_{12}(bpy). Reprinted with permission from ref 70. Copyright (2017) Springer Nature. (f) Chiral gold quartet framework exhibits dynamic structural change, leading to reversible luminescence response when subjected to vacuum and subsequently gas exposure. Reprinted with permission from ref 73. Copyright (2019) Elsevier.

reactant chemisorption is primarily determined by nanoscale interactions between the adsorbent and the adsorbate. Catalytic activity is heavily dependent on such interaction and, according to Sabatier Principle, is maximized at the optimum when the interaction is neither too strong nor too weak. In the case of Au NCs, their drastic difference in catalytic performance compared with their bulk counterpart is an example of the significance of this interaction. Typically, the surface atoms of bulk gold require high ionization energy to yield d-band vacancy for interaction with molecules of other elements.[74] Moreover, the interaction between these high-coordination atoms and O, for example, is suppressed by its neighbors.[75] However, for nanogold, the surface atoms with low coordination number can actively form stronger interactions with O.[76] Moreover, metal NCs also feature an atomically precise structure that can be customized and probed at ∼1 Å resolution. Therefore, these metal NCs with larger surface-to-volume ratios, more low-coordinated surface metal atoms, and resolved structural information build a delicate platform where fundamental questions such as surface

https://doi.org/10.1021/prechem.4c00044
Precis. Chem. 2024, 2, 495−517

structure, active sites, reaction mechanism, and structure–property relationship can be quantitatively and qualitatively answered at the unprecedented molecular and atomic levels.[77]

For metal NCs, catalytic reactions often occur on the accessible metal atoms located on the surface of the metal core or in metal–ligand motifs. As these NCs require surface passivation for structural stability, their surface ligands also play a part in their catalytic performance. On one hand, their steric effect may hinder the access of reactants to the active site.[78] On the other hand, they may construct a unique chemical environment that promotes reaction activity or selectivity for selected reactions.[79,80] This section discusses the strategies of tailoring electronic structures and accessibility of active sites of metal NCs for better catalytic performance by leveraging on molecular interactions. Of note, recent advances also suggest that coadsorbed "co-factors" can affect the selectivity of metal NCs, which is also deciphered in this section.

4.1. Tailoring Electronic Structure for Optimal Adsorption

Like other heterogeneous catalysts, a metal NC starts its catalysis with a crucial adsorption step. Moderate strength is optimal to balance the energy barrier against surface adsorption and the desorption of reactants and products. With their structure solved, metal NCs allow quantification of adsorption strength by calculating the electronic structures of metal NCs and of adsorbed reaction intermediates. The d-band distribution and the relative position of the d-band center with the Fermi level can therefore be calculated as the indicator of the strength of this adsorbent–adsorbate interaction.[81] This explains the higher activity of low coordination surface metal atoms. As a result, electronic structure tailoring can directly modify the adsorbent–adsorbate interactions and the catalytic activity of the material. Numerous factors, such as metal core size, structure, doping, and choice of ligands, can influence such interactions via electronic structural differences, with metal core size being one obvious example for its close correlation with coordination numbers of surface atoms.[82,83]

Zhang et al. reported an increasing trend of catalytic activity with decreasing size of MPA-protected Au NCs in resazurin reduction by NH_2OH (MPA refers to 3-mercaptopropionic acid).[82] This observation could be explained by their DFT result that increasingly stronger adsorption of the substrate and weaker adsorption of the product were observed as the cluster size decreased. However, the size factor is complex and most probably reaction specific, as other trends, such as volcano-shaped and size-independent ones, were reported as well.[84,85] More research effort is required to simplify the question further for more insight.

Heteroatom doping is another commonly used measure for adjusting the electronic structure of the catalyst. The heteroatoms or dopants can be located on the surface or in the core of the NCs. In terms of surface modification, the surface doped bimetallic $Au_{24}Ag_{46}$ supported on carbon nanotube ($Au_{24}Ag_{46}$/CNT, CNT refers to carbon nanotubes) simultaneously exploited the high conversion of Au and high selectivity for benzaldehyde of Ag in styrene oxidation.[86] It was reported with higher conversion than Ag_{44}/CNT and higher selectivity for benzaldehyde than Au_{25}/CNT. When the comparison of catalytic performance was further made between the surface-doped and central-doped NCs, the central-doped $Ag_{32}Au_{12}$/CNT showed lower selectivity for benzaldehyde (Figure 6a). In a recent example, the effect of central doping

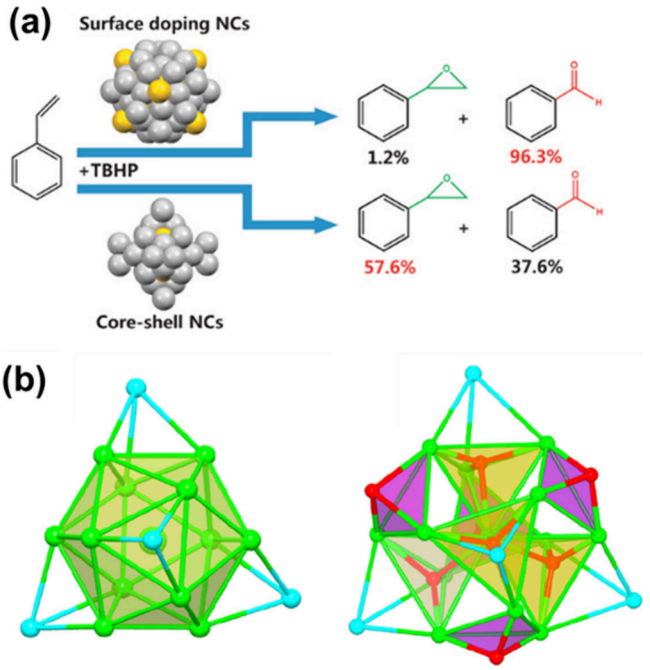

Figure 6. Schematic illustrations of (a) surface-doped bimetallic $Au_{24}Ag_{46}$ NCs and central-doped $Ag_{32}Au_{12}$ NCs having different catalytic performances for the oxidation of styrene. Gray, silver; yellow, gold. Reprinted with permission from ref 86. Copyright (2015) American Association for the Advancement of Science. (b) Metal core of $Ag_{13}Cu_4$ (left) and twisted metal core of $Ag_{13}Cu_4H_8$ (right). Green, Ag; blue, Cu; red, H. Reprinted with permission from ref 87. Copyright (2022) American Chemical Society.

on the catalytic performance of NCs is explained.[87] The additional 8 H in the core of $Ag_{13}Cu_4H_8$ resulted in an electron-deficient core with only Ag(I) and Cu(I) (Figure 6b). In comparison, the undoped $Ag_{13}Cu_4$ was found with an electron-rich core with eight valence electrons. As the authors proposed the reaction rate was dictated by the adsorption and B–H bond cleavage of $[BH_4]^-$, the H-doped cluster can better interact with the negatively charged $[BH_4]^-$, resulting in its marked activity enhancement in 4-NP hydrogenation to 4-AP with a conversion increase from ~8% to 100%.

Similarly, single-atom central doping can also induce a more positively charged surface. When the central Ag atom of Ag_{25} NCs was replaced by Au/Pt/Pd atoms to form $M@Ag_{24}$ NCs,[88] its catalytic activity in the carboxylation of CO_2 with terminal alkyne into propiolic acid was changed (Figure 7a). The existing central dopant induced electron donation from Ag, leaving surface Ag more positively charged. The reduced electron density facilitated the adsorption of the electron-rich alkyne and desorption of the product. The most significant electron donation from Ag to Au endowed $Au@Ag_{24}$ with superior activity among all. Moreover, single atom central doping of Pt to $Au_{25}(SC_6H_{13})_{18}$, where SC_6H_{13} stands for 1-hexanethiolate, changed the superatomic electronic configuration from 8 e^- to 6 e^- and led to a Jahn–Teller-like distortion of the metal core and a split of the 1P orbital (Figure 7b). As such, the reduction potentials of $[PtAu_{24}]^0$ were more positive and matched well with the thermodynamic potential of a proton.[89] This was supported by the DFT result, in which hydrogen adsorption to $[PtAu_{24}]^{2-}$ was nearly thermodynamically neutral. In conclusion, doping is a usual tool to design NC

https://doi.org/10.1021/prechem.4c00044
Precis. Chem. 2024, 2, 495–517

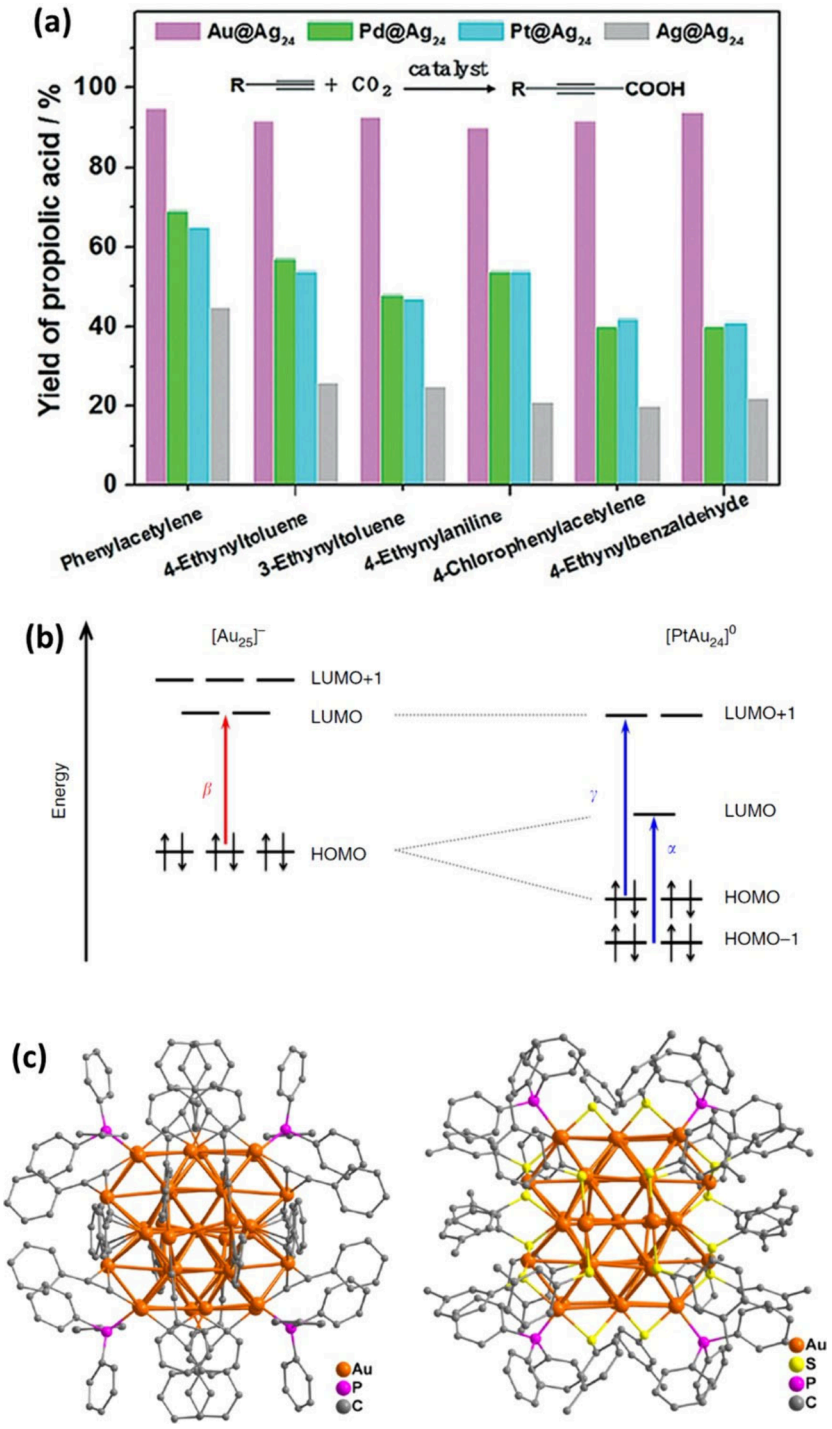

Figure 7. (a) Catalytic performance of Au/Pd/Pt/Ag@Ag_{24} in carboxylation of a terminal alkyne with CO_2. Reprinted with permission from ref 88. Copyright (2018) Wiley. (b) Electronic energy levels of $[Au_{25}]^-$ and $[PtAu_{24}]^0$. β denotes the optical absorbance at 690 nm (1.8 eV) for $[Au_{25}]^-$. α denotes the optical absorbance at 1130 nm (1.1 eV), and γ at 590 nm (2.1 eV) denotes the optical absorbance for $[PtAu_{24}]^0$. Reprinted with permission from ref 89. Copyright (2017) Springer Nature. (c) Atomic structures of alkynyl (left) and 3-methylbenzenethiol (right) protected Au_{38} NCs. Reprinted with permission from ref 90. Copyright (2017) American Association for the Advancement of Science.

catalysts by tinkering with the electronic structures of active metal core.

The choice of surface ligand can also affect NC's electronic structure and, thus, catalytic performance. Metal NCs with the same metal core structure but different types of protective ligands were studied by Wang and co-workers.[90] Two isostructural Au_{38} molecules protected by either alkynyl (PhC≡C) or thiolate (3-methylbenzenethiol), as illustrated by Figure 7c, possessed different electronic structures as shown by distinct UV−vis spectra. Meanwhile, the alkynyl-capped Au_{38} supported on TiO_2 was evidently more active (conversion >97%) than the thiolate-capped one which was nearly inactive (conversion <2%) in semihydrogenation of alkynes. This was explained by the electronic structure of alkynyl-capped Au_{38} NCs, which was indicated to be more suitable for the adsorption and dissociation of H_2 on the cluster. Additionally,

https://doi.org/10.1021/prechem.4c00044
Precis. Chem. 2024, 2, 495−517

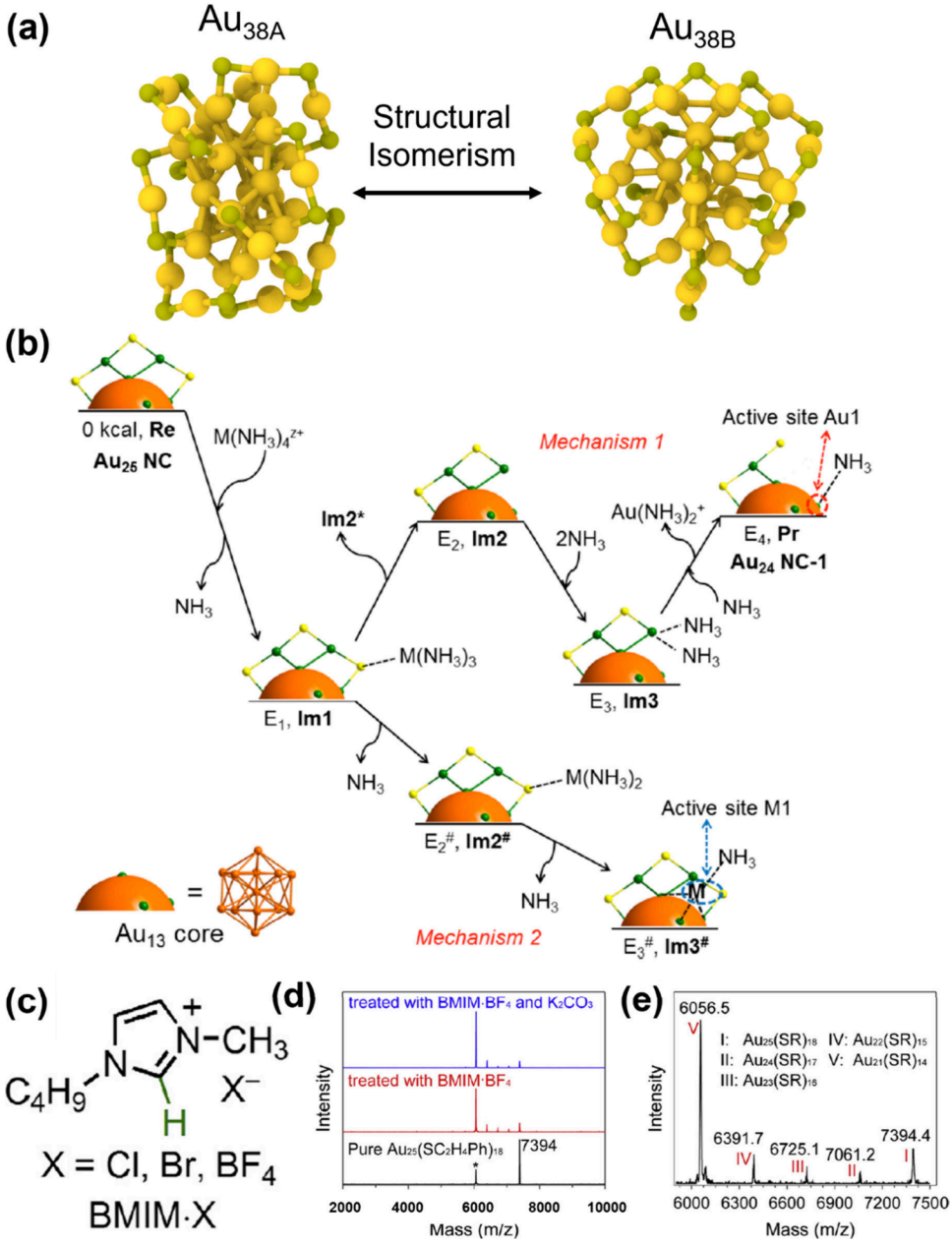

Figure 8. (a) Isomerization occurs between Au_{38Q} (left) and Au_{38T} (right). The molecular formula for the two isomers is $Au_{38}(PET)_{24}$. Yellow, gold; green, sulfur. (b) Proposed mechanisms for ligand removal of $Au_{25}(SR)_{18}$ (Mechanism 1) and formation of adduct $[NC\text{-}M]^{(z-1)+}$ (mechanism 2) in the presence of metal cations M^{z+} and ammonia. Reprinted with permission from ref 99. Copyright (2015) American Chemical Society. (c) Molecular structure of imidazolium-based ionic liquids used for promoting Suzuki cross-coupling reaction. (d) MALDI mass spectra of the original $[Au_{25}(SR)_{18}]^-$ (bottom) and those after treatment with BMIM·BF_4 (middle) or with BMIM·BF_4 and K_2CO_3 (top). (e) Enlarged view of the MALDI mass spectrum of the sample after treating $[Au_{25}(SR)_{18}]^-$ with BMIM·BF_4. Panels c–e are reprinted with permission from ref 100. Copyright (2016) Elsevier.

peroxidase-like activity of Au_{15} protected by different thiolate ligands was evidenced differently by Xie and co-workers. The main reason was computationally ascribed to the electron density around the Au atoms in the surface motifs.[91] As compared to the control group $Au_{15}(MPA)_{13}$, the electron-withdrawing effect of NAC (NAC refers to *N*-acetylcysteine) lowered the energy barrier of H_2O_2 dissociation on $Au_{15}(NAC)_{13}$, while the electron-donating effect of MMPA raised that barrier (MMPA refers to 3-mercapto-2-methyl-propanoic acid).

4.2. Improving Active Site Accessibility

Surface ligands play a significant role in the formation of ultrasmall metal NCs. They provide protection around the metal core and are critical to cluster stability.[92] However, these protective ligands can often negatively affect the accessibility of the metal active sites on the surface of the metal NCs. These ligands can hurdle the diffusion of substrates or block the active sites and limit the formation of adsorbent–adsorbate interactions, restraining the cluster's catalytic activity. Sometimes, the catalytic process must be initiated with a ligand removal step.[93] Thus, to improve the availability of active sites,

https://doi.org/10.1021/prechem.4c00044
Precis. Chem. 2024, 2, 495–517

strategies like the use of less bulky ligands, and partial or complete ligand removal, have been reported effective.[77,94,95] Moreover, NCs with labile metal−ligand bonds which are more prone to cleavage have also been developed.[96]

For isostructural metal NCs, the choice of less bulky ligands can facilitate the diffusion of the substrate. In the case of 4-nitrophenol (4-NP) hydrogenation to 4-aminophenol (4-AP) catalyzed by $Au_{25}(SR)_{18}$, the longer the ligand carbon tail and the stronger hydrophobic interactions among the ligands, the harder the diffusion of reactant, as indicated by the reaction induction time.[78] In addition to the carbon tail length, functional moieties of protecting ligands are found to be another important attribute dictating the catalytic performance of metal NCs in the same report by Li et al. When the functional group of the ligands was altered to the zwitterionic cysteine, pseudocage-like structures could be formed by intramolecular electrostatic interactions and H-bonding, preventing the access of the metal core to the reactants. Of note, ligand−reactant interactions like $\pi-\pi$ interactions between the *p*-MBA ligands of NCs and 4-NP in this study could facilitate reactant adsorption but may hamper the desorption process. Similarly, the steric effect of the ligand shell in hampering the access of reactants has also been documented. A structural isomer pair of Au_{38Q} and Au_{38T} (Figure 8a) protected by the same ligand (PET or phenylethanethiolate ligand) were reported to have distinctly different activities in 4-NP reduction to 4-AP.[97] Under the same condition, Au_{38T} was reported active while Au_{38Q} was inactive, which was probably attributable to the less passivation of the Au_{38T} surface. However, the extent of passivation for these two isomers is not quantitatively accessed, which may require future computational efforts.

One strategy to improve the accessibility of active sites is ligand removal. Thermal ligand removal has been widely used to break off some or all ligands for catalytic investigations of metal NCs.[77] For example, Tsukuda and co-workers found that the activity of $Au_{25}(SR)_{18}$ in the aerobic oxidation of benzyl alcohol was enhanced by ligand removal.[94] However, this measure usually introduces complications and difficulties in studying the effect of molecular interactions in details. First, external supports are usually required to maintain the intactness of the metal core during the thermal treatment. As some supports can participate in the reaction, the reaction is complicated by support−NC and support−substrate interactions.[95,98] Moreover, rearrangement and sintering of metal atoms on the support may occur, the degree of which is hard to characterize at the atomic level at the current stage.

A more subtle way is to utilize the interaction of NCs with "promoters" to achieve partial ligand removal. These promoters can interact with the NCs and facilitate the cleavage of surface motifs for active site exposure. For instance, transition metal cations functioned as Lewis acids which promoted catalytic benzaldehyde hydrogenation of unsupported and CeO_2-supported $Au_{25}(SR)_{18}$ ($Au_{25}(SR)_{18}/CeO_2$) via ligand removal (Figure 8b).[99] The control group using unsupported $Au_{25}(SR)_{18}$ was almost inactive. However, upon the addition of Co^{2+} ions, the conversion was increased from 13.4% to 90.1% using $Au_{25}(SR)_{18}/CeO_2$. Ligand-removed NCs including $[Au_{24}(SR)_{17}]^-$ and those with metal adducts were observed in the mass spectrum. The effect of transition metal cations on ligand removal was supported by DFT calculations, as the bond formation between a transition metal ion and sulfur was found to be very exothermic, which in turn would facilitate the removal of the Au−S fragment. Two reaction mechanisms and three possible active sites were proposed based on DFT results. Unfortunately, no further evidence was found to narrow down the scope or identify the most prominent active site. In another work by Jin and co-workers, imidazolium-based ionic liquid was found as an "activator" in Suzuki cross-coupling reaction between phenylboronic acid and *p*-iodoanisole by using $Au_{25}(SR)_{18}$ supported on TiO_2 as catalysts.[100] Ionic liquid BMIM·X (BMIM denotes 1-butyl-3-methylimidazolium and X denotes anions such as Cl, Br, and BF_4) promoted the reaction from less than 0.5% conversion without any promoters to above 89%. The acidic hydrogen atom at position 2 of imidazolium ions was identified as the key contributor to catalytic enhancement via the removal of Au-SR from the motifs for active site exposure (Figure 8c, 8d, and 8e). BMIM's effectiveness in ligand removal was supported by theoretical calculations. With the increasing understanding of the molecular interactions between NCs and other molecules, it is expected that more and more "activators" will be discovered to help speed the reactions catalyzed by metal NCs.

Another notable strategy for easy ligand removal is the introduction of a moderate metal−ligand bond. Wang et al. reported a novel Au NC that can be readily activated by $NaBH_4$ to achieve almost 100% conversion with above 90% *Z*-alkene selectivity in the semihydrogenation of alkynes.[96] In their work, the newly discovered $[Au_{11}Cl_2(dppee)_4]^+$ had labile bonds with Cl^- ligands which could readily exchange with a hydride from $[BH_4]^-$ and form $[Au_{11}HCl(dppee)_4]^+$ (dppee refers to bis(2-diphenylphosphino)ethyl ether). The activated cluster species easily underwent a hydroauration reaction with polarized alkynes. The reaction mechanism was proposed with key reaction intermediates, namely, $[Au_{11}(BH_4)Cl(dppee)_4]^+$ and $[Au_{11}HCl(dppee)_4]^+$, identified and characterized using ESI-MS and NMR (Figure 9a). Of note, this hydride did not change the electronic structure of the core as indicated by UV−vis signals. The significance of the bonded hydride was confirmed by the inertness of the metallic hydrogen bonded $[Au_9H(PPh)_8]^{2+}$ NC. In another example, $Au_{25}(S\text{-}Nap)_{18}$ (S-Nap refers to 1-naphthalenethiolate) exhibited superior performance in catalyzing Ullmann heterocoupling between 4-methyliodobenzene and 4-nitro-iodobenzene, compared to $Au_{25}(SCH_2CH_2Ph)_{18}$ and $Au_{25}(SCH_2CH_3)_{18}$ which share similar structures and UV−vis spectra. Bonds between aromatic ligand S-Nap and Au cores were found relatively weaker which was ascribed to the better capability of aromatic ligands in stabilizing the electrons of S via π-resonance.[101] As a result, the aromatic ligand-Au bond could be cleaved to form the active species $Au_{25}(SR)_{18-x}$ (where x = 1 or a few) more easily. To conclude, NCs may be purposely designed with weak metal−ligand bonds, which can promote the accessibility of active sites for incoming reactants.

However, the absence of ligands is not desirable in certain cases. The steric effects of protective ligands can sometimes be utilized. During 4-NP hydrogenation, unlike the very open active sites on the naked nanogold catalyst surface, simultaneous adsorption of two 4-nitrophenol molecules and one $[BH_4]^-$ on the Au_3 active site was confined in the space limited by surface ligands of $Au_{25}(p\text{-}MBA)_{18}$ (Figure 9b). This facilitated semihydrogenation forming cis isomer of 4,4′-dihydroxyazobenzene intermediate via a new catalytic pathway, as reported by Nasaruddin et al. The benzene rings of *p*-MBA also facilitated the adsorption and containment of 4-nitro-

https://doi.org/10.1021/prechem.4c00044
Precis. Chem. 2024, 2, 495−517

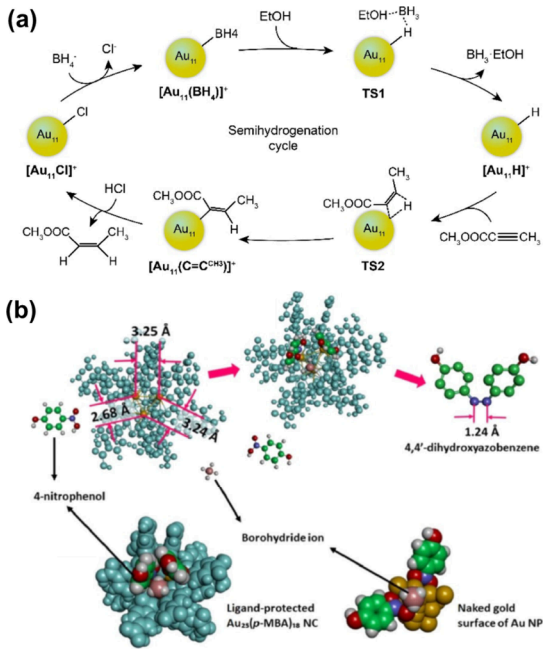

Figure 9. (a) Schematic illustrations of the reaction pathway of $[Au_{11}Cl_2(dppee)_4]^+$ in semihydrogenation of alkynes to form the *Z*-alkene product. Reprinted with permission from ref 96. Copyright (2022) American Chemical Society. (b) Schematic illustrations of adsorption of 4-nitrophenol and a borohydride ion on $Au_{25}(p\text{-MBA})_{18}$ and naked gold. Reprinted with permission from ref 80. Copyright (2018) Wiley.

benzene via $\pi-\pi$ stacking interactions.[80] This example illustrates ligands' steric effect in regulating the catalytic reaction path.

4.3. Simultaneous Modification of Electronic Structure and Steric Effect

Interestingly, the above-mentioned two enhancement effects can be achieved simultaneously. Efforts have been devoted to designing and synthesizing metal NCs with more exposed and low-coordinated metal atoms available for catalytic activities. Several successful attempts were reported using bulky ligands.[102,103] In a recent work by Li et al.,[104] $Au_{43}(C{\equiv}C^tBu)_{20}$ which has an apical Au atom coordinated to no ligand was successfully synthesized (Figure 10a) ($C{\equiv}C^tBu$ stands for 3,3-dimethyl-1-butynyl). Without ligand removal, this NC supported on Al_2O_3 exhibited higher conversion in benzyl alcohol oxidation than NC species without such uncoordinated gold atoms. When Ag was doped at the apical position, the conversion was significantly affected. This was partially caused by the shorter Ag−Au bond, which hindered the availability of this site according to topological studies (Figure 10b and 10c). Of note, the author also pointed out the electronegativity of H being smaller than Au but larger than Ag, and the partial positive charge of Ag would contribute to the catalytic difference. The synergistic effect of suitable electronic structure and exposure of active sites endows $Au_{43}(C{\equiv}C^tBu)_{20}$ NCs with more favored adsorption for benzyl alcohol and enhanced catalytic performance. In another example, adamantanethiolate ligand-protected $Au_{36}Ag_2(SR)_{18}$ with open surface and low-coordinated core metal atoms with notable performance in electrocatalytic hydrogen evolution reaction (HER) was reported by Jin and co-workers (Figure 11a and 11b).[105] The core Au atoms, whose coordination number is lower than those of $Au_{38}(SR)_{24}$ and $[Au_{25}(SR)_{18}]^-$, were found as the most feasible active sites for H adsorption. It possessed the lowest H binding energy among the three NCs, despite adverse effects imposed by full ligation and bulkier protective ligand, as shown by DFT calculations.[106] In terms of site accessibility, its active sites were more exposed, as supported by its much higher electrochemically active surface areas among the three NCs. Of note, its higher electron affinity contributed to its high activity in the HER by allowing more energetically favorable electron transfer during the Volmer step, a step where protons are adsorbed onto electrodes at the same time.

Besides the use of bulky ligands, Zheng and co-workers reported $[Au_{16}(NHC)_5(PA)_3Br_2]^{3+}$ NCs whose more accessible Au in the surface motif functioned as the adsorption site while Au atoms in the core as the reaction site in the hydroamination of alkynes (PA refers to phenylacetylide and NHC refers to N-heterocyclic carbene).[107] Upon the successful capture of reaction intermediates, a reaction

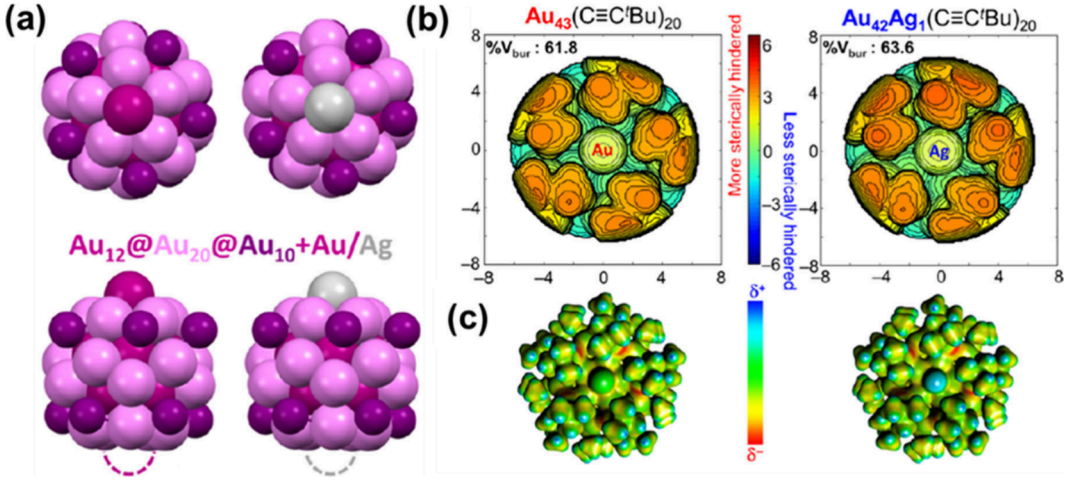

Figure 10. (a) Illustration of core structures of $Au_{43}(C{\equiv}C^tBu)_{20}$ and $Au_{42}Ag_1(C{\equiv}C^tBu)_{20}$, emphasizing the one coordinatively unsaturated Au or Ag atom on the Au_{20} shell, and the location of the vacancy is indicated by the dashed circle. Magenta/violet/purple, gold; light gray, Ag. (b) Topographic steric hindrance maps and (c) electrostatic potential maps of (left) $Au_{43}(C{\equiv}C^tBu)_{20}$ and (right) $Au_{42}Ag_1(C{\equiv}C^tBu)_{20}$. Panels a−c are reprinted with permission from ref 104. Copyright (2023) American Chemical Society.

https://doi.org/10.1021/prechem.4c00044
Precis. Chem. 2024, 2, 495−517

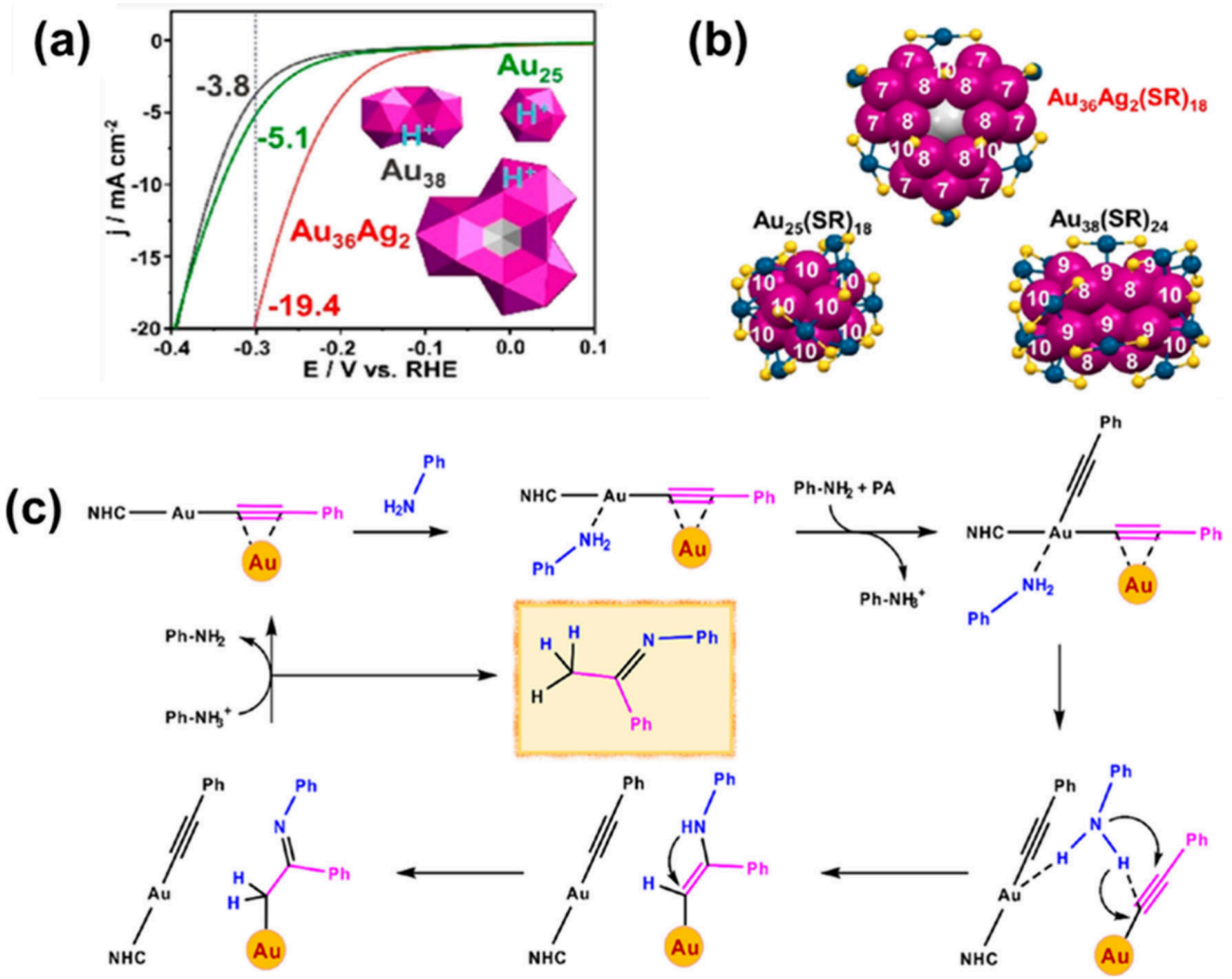

Figure 11. (a) HER voltammograms of $Au_{36}Ag_2(SR)_{18}$, $[Au_{25}(SR)_{18}]^-$, and $Au_{38}(SR)_{24}$ NC catalysts. (b) The coordination numbers of Au atoms on the core's surface of $Au_{36}Ag_2(SR)_{18}$, $[Au_{25}(SR)_{18}]^-$, and $Au_{38}(SR)_{24}$. Magenta, kernel Au; light gray, Ag; yellow, S; navy, motif Au. Panels a and b are reprinted with permission from ref 105. Copyright (2021) American Chemical Society. (c) Reaction mechanism showing the synergistic effect of Au atoms on the surface motif and in the core in hydroamination of alkynes. Reprinted with permission from ref 107. Copyright (2022) American Chemical Society.

mechanism was proposed (Figure 11c). When mere organometallic molecules or Au_{13} NCs that possessed the same core structure without surface motifs were tested, no reaction was observed. Hence, such a synergistic effect of metallic core and motifs was further confirmed. Such delicate use of motif−core synergy should be further explored to pave new paths in NC catalyst designs.

4.4. Introduction of "Cofactors"

In the field of biology, cofactors interact with enzymes through molecular interactions and change their catalytic properties. Similar to the cofactor in enzymatic reactions, appropriate small molecules can form an integrated structure with NCs and alter the reaction performance. In the selective oxidation of styrene catalyzed by Au_{25}/CNT, when a trace amount of water was added to the pure toluene, selectivity shifted to benzaldehyde rather than epoxide.[108] As more water was added, the selectivity of benzaldehyde increased (Figure 12a and 12b). As shown in FT-IR spectra (Figure 12c and 12d), a band centered at ∼1630 cm^{-1} was identified and assigned to the δ_{OH} of coadsorbed water, while the XPS result indicated little difference in the Au $4f_{7/2}$ binding energy with or without water. Thus, the authors concluded that the water present neither changed the valence state of Au nor reacted with an epoxide to form benzaldehyde. Instead, it was hypothesized that the water adsorbed onto the surface of Au_{25}, and a reaction mechanism was proposed with the assistance of DFT calculations. Upon adsorption, water interacted with the oxidant *tert*-butyl hydroperoxide (TBHP) and preferentially formed benzaldehyde. This was supported by an isotopic experiment using $^{18}OH_2$, where ^{18}O was found in the product. However, few reports are available on the coadsorption of small molecules for metal NCs in catalysis. More studies and discussions are required for further insights.

In summary, the adsorbent−adsorbate interaction is heavily dependent on the electronic structure of metal NCs, the accessibility of the active site, and the coadsorption of other molecules. Multiple effects can also be utilized in tandem to tailor the catalytic performance of the metal NCs. Of note, many observations made so far are reaction specific. Moreover, as the field of NC-based catalysis is growing at an accelerated pace, many fundamental issues are expected to be solved in the near future. For example, active sites in many reactions are under debate and remain elusive.[109,110] Difficulty in intermediate capture also impedes reaction mechanism

https://doi.org/10.1021/prechem.4c00044
Precis. Chem. 2024, 2, 495−517

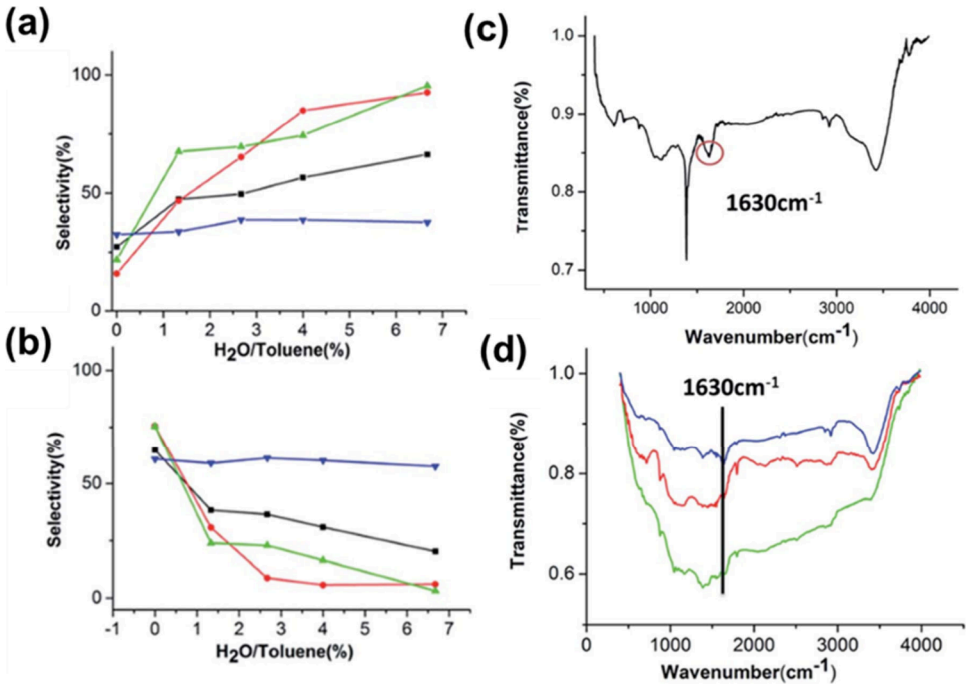

Figure 12. (a) Benzaldehyde selectivity and (b) epoxide selectivity as functions of the volume percent of water in the selective oxidation of styrene catalyzed by bimetallic NCs. Black line, Au_{25}/CNT; red line, $Au_{25-x}Ag_x$/CNT; cyan line, Ag_{44}; and blue line, $Au_{12}Ag_{32}$/CNT. FT-IR spectra of catalysts soaked with water: (c) $Au_{25-x}Ag_x$/CNT and (d) Ag_{44}/CNT (blue line), Au_{25}/CNT (red line), and $Au_{12}Ag_{32}$/CNT (green line). Panels a–d are reprinted with permission from ref 108. Copyright (2016) Royal Society of Chemistry.

determination in order to facilitate and cross-refer with theoretical predictions. Furthermore, on many occasions, there is a lack of appropriate NCs to build a simple control group for investigation. Therefore, future efforts on active site determination, intermediate characterization, and expansion of the metal NC library for more systematic and rational design are highly desirable to enhance the metal NC catalytic activities.

5. COMPETING FORCES IN SELF-ASSEMBLY

To diversify the practical applications of metal NCs such as catalytic or optical applications, self-assembly provides an alternative means other than the size and structure engineering of an individual cluster. While the quantitative structure–activity relationship (QSAR) between these properties and NC arrangements might be one crucial principle guiding the design of assembled NC architectures, this section focuses on another question: how a desirable structure can be assembled by various molecular forces, such as hydrogen bonding, ionic interaction, and metallophilic interaction. Through a brief discussion on several demonstrative examples, this section aims to convince readers that precise structural engineering of assembled NC architectures can be made possible by delicate manipulation of competing supramolecular interactions in the self-assembly process.

For self-assembly, the hydrophilicity or hydrophobicity of NCs that is often determined by the terminal functional group of ligands plays a significant role. For hydrophilic NCs, dialysis is a common technique for inducing self-assembly,[51,111] while for the hydrophobic NCs, vapor diffusion, antisolvent diffusion or even natural evaporation can be used to produce high-quality crystals.[8,112,113] Hence, in this section, the discussion is split into two parts according to the hydrophilicity or hydrophobicity of the NCs. Hopefully, more quantitative predictive theory can be developed for researchers to rationally design and manufacture nanoscopic building blocks.

5.1. Intracluster and Intercluster Ligand Interaction for Hydrophobic NCs

Intracluster and intercluster ligand interaction is one of the most important forces in self-assembly. As metal NCs are protected by a layer of ligands, the interactions between the ligand bodies or between the terminal functional groups will determine the morphology of the resulting assembly. For instance, when the ligands do not possess enough kinetic energy to overcome the attractive van der Waals forces between the ligand body formed by carbon tails, orderly bundles of ligands might form. The shape and the position of the thus-formed ligand layer will either promote or hinder the formation of certain self-assembly structures. $[Au_4Pt_2(SR)_8]^0$ NCs were used as a building block for self-assembly to demonstrate the relationship between ligand structure and ligand interaction.[112] In Figure 13, SCH_2PhCl (iv) and SC_2H_4Ph (v) had smaller repulsive intracluster ligand forces compared to $SCH(CH_3)_2$ (i), $SCH_2Ph(CH_3)_3$ (ii), and SCH_2Ph^tBu (iii), as iv and v did not possess bulky alkyl groups, where SCH_2PhCl denotes 2-chlorobenzenemethanethiol, SC_2H_4Ph denotes 2-phenylethanethiol, $SCH(CH_3)_2$ denotes 2-propanethiol, $SCH_2Ph(CH_3)_3$ denotes 2,4,6-trimethylbenzylmercaptane, and SCH_2Ph^tBu denotes 4-*tert*-butylbenzylmercaptane. This competition between attractive ($\pi-\pi$ interaction) and repulsive forces (steric hindrance) led to compact or spread ligand layers. Consequently, strong $\pi-\pi$ interaction was allowed to occur between adjacent clusters by a slight rotation in cluster orientations for iv and v, while bulky groups on i, ii, and iii distance clusters away from adjacent ones. Hence, one-dimensional assembled structure was only obtained for ligands iv and v, which allowed for aurophilic interaction between NCs within a shorter distance around 3 Å

https://doi.org/10.1021/prechem.4c00044
Precis. Chem. 2024, 2, 495–517

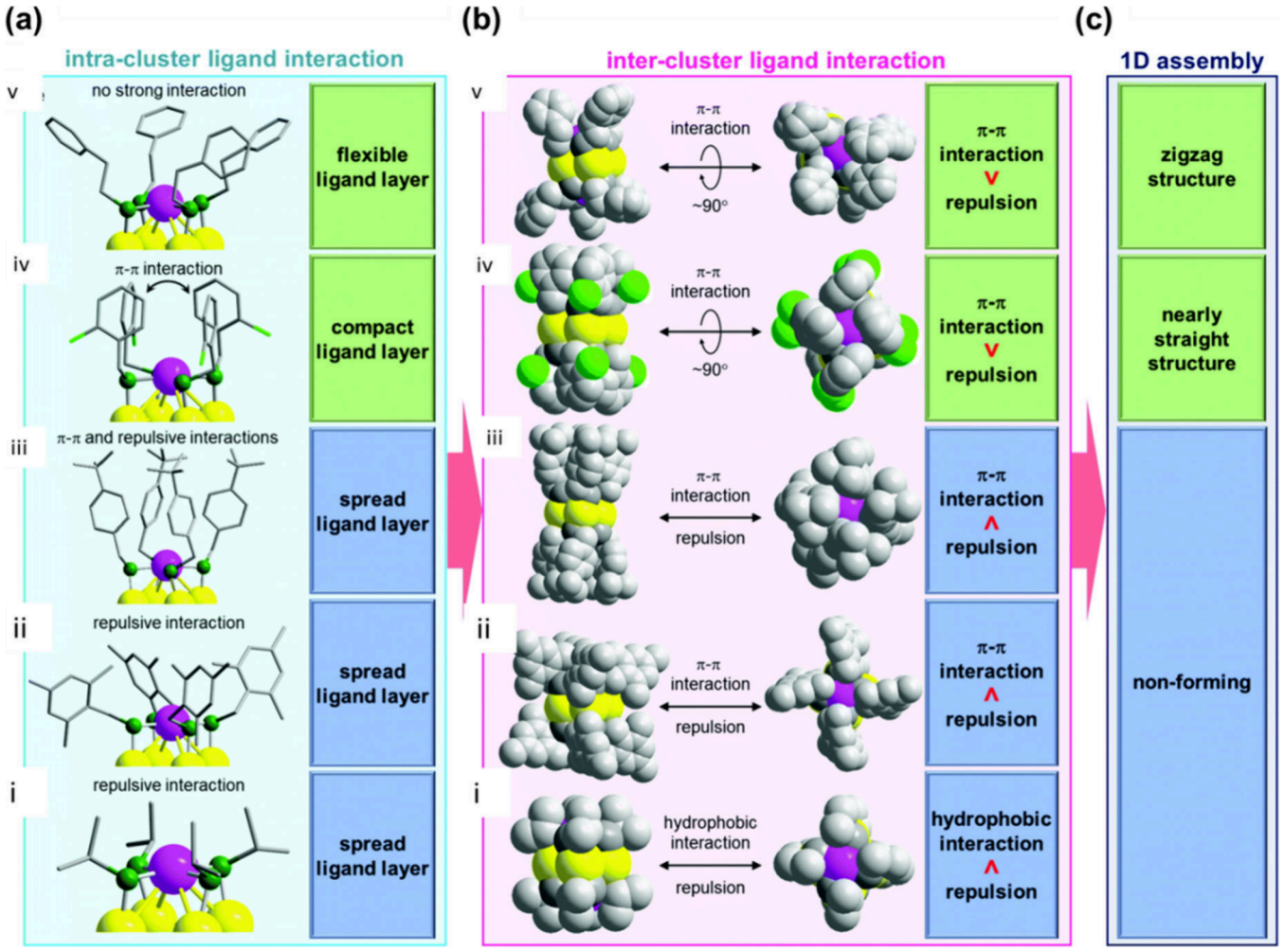

Figure 13. Schematic illustrations of the influence of intracluster and intercluster ligand interaction on the 1D assembly of $[Au_4Pt_2(SR)_8]^0$ NCs. (a) The compactness of ligand layer is determined by the type of ligands and the relative strengths of repulsion and attraction. (b) Relative strength between $\pi-\pi$ interaction and repulsive steric hindrance determines the distance between NCs in their assembled form, and (c) 1D assembly for i−v. Light gray, carbon chain; green, sulfur; purple, platinum; yellow, gold. Panels a−c are reprinted with permission from ref 112. Copyright (2020) Royal Society of Chemistry.

in contrast to more than 5 Å or even 10 Å for i−iii. However, the authors also pointed out that due to the difference in metal core size, using similar ligands for larger NCs may not yield similar one-dimensional self-assembly. In addition, repulsive forces between ligands may be desirable in forming certain desirable assembly. For instance, a dimer with a precise formula of $Ag_2Au_{50}(PET)_{36}$ could be assembled from $Au_{25}(PET)_{18}$ and its further integration with more monomers was prohibited by the steric hindrance of four protruded benzene rings.[114]

One of the common structural consequences resulting from a delicate balance of attractive and repulsive behavior in self-assembly is the interlocking behavior of ligands, where the ligand shells of two NCs intersect and ligands are locked in position. This interdigitation of ligands often occurs for benzene-containing NCs (Figure 14a, 14b, and 14c).[8,115,116] The abundance of CH···π interactions or $\pi\cdots\pi$ stacking might be the reason for the close packing. Take $Au_{103}S_2(S\text{-}Nap)_{41}$ as an example. Two naphthalene rings formed a T-shaped structure (Figure 14c). This interligand interaction further formed a tetramer and finally a needle-like one-dimensional crystal. However, the relationship between isolated and assembled NCs might not be described simply as interdigitation since structural changes might occur during self-assembly. In a report by De Nardi et al.,[117] one antiferromagnetic structure composed of $[Au_{25}(SBu)_{18}]^0$ was discovered. In contrast to the inability of $[Au_{25}(SEt)_{18}]^0$ to form a one-dimensional polymer, $[Au_{25}(SBu)_{18}]^0$ polymerization was facilitated by a phenomenon termed "twist and lock" by the authors (SEt denotes ethanethiolate, and SBu denotes *n*-butanethiolate). As shown in Figure 14d, the bond distance between the motif gold and the gold on the core surface was elongated to 3.369 Å. This deformation combined with the twist and turn of NCs and strong dispersion forces between ligands led to the formation of gold nanowires. Hence, it is important to treat the resolved NC structure carefully, as the competing intermolecular forces during self-assembly might deform the atomic arrangement. In addition to self-assembly, more observation on the surface interaction and metal core structure from other aspects can be found in section 3.

Complex hierarchical structures like nanowires or layered systems, or even helical structures can also arise from the competing intracluster and intercluster interactions.[117−119] In 1962, the Nobel Prize was awarded to the discovery of a

https://doi.org/10.1021/prechem.4c00044
Precis. Chem. 2024, 2, 495−517

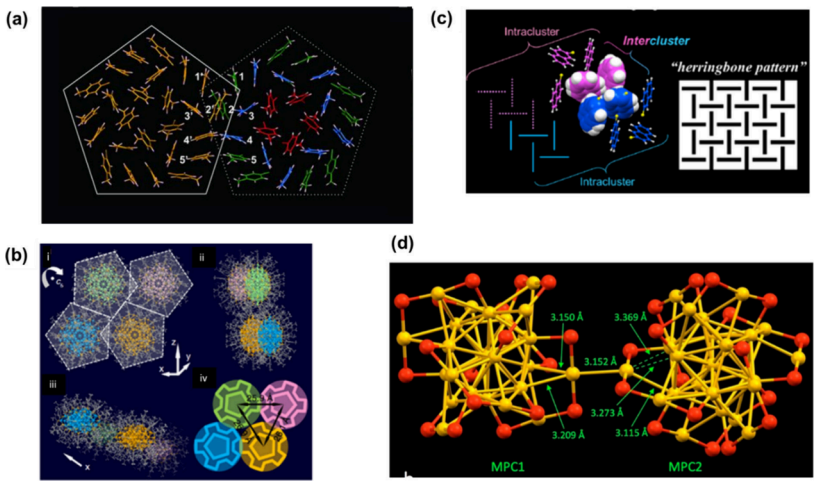

Figure 14. (a) Packing structures showing the interdigitation of Au_{246}(*p*-MBT)$_{80}$ (*p*-MBT denotes *p*-methylbenzenethiolate). Self-assembly is dictated by the density of ligands and surface symmetry. Side-by-side stacking of the ligands is shown. The dotted lines enclose one NC, and only *p*-MBT ligands are shown. Reprinted with permission from ref 8. Copyright (2016) American Association for the Advancement of Science. (b) The assembly of $[Cu_{72}Au_{52}(SR)_{55}]^+$. (i) Four NCs interact and pack closely. View of four NCs from side (ii) and top (iii). (iv) Simplified diagram showing the interlocking behavior. Green/pink/blue/yellow, metal core; white, ligands. Reprinted with permission from ref 115. Copyright (2020) Springer Nature. (c) Structures of interacting ligands between two NCs in the assembly. Combination of intercluster and intracluster ligand interactions forms a T-shaped structure or "herringbone pattern". Blue/pink, C; white, H. Reprinted with permission from ref 116. Copyright (2017) American Chemical Society. (d) Stick-and-ball view of the $Au_{25}S_{18}$ dimer that was in the $Au_{25}(SBu)_{18}$ assembly. Au, yellow; S, red. Reprinted with permission from ref 117. Copyright (2022) American Chemical Society.

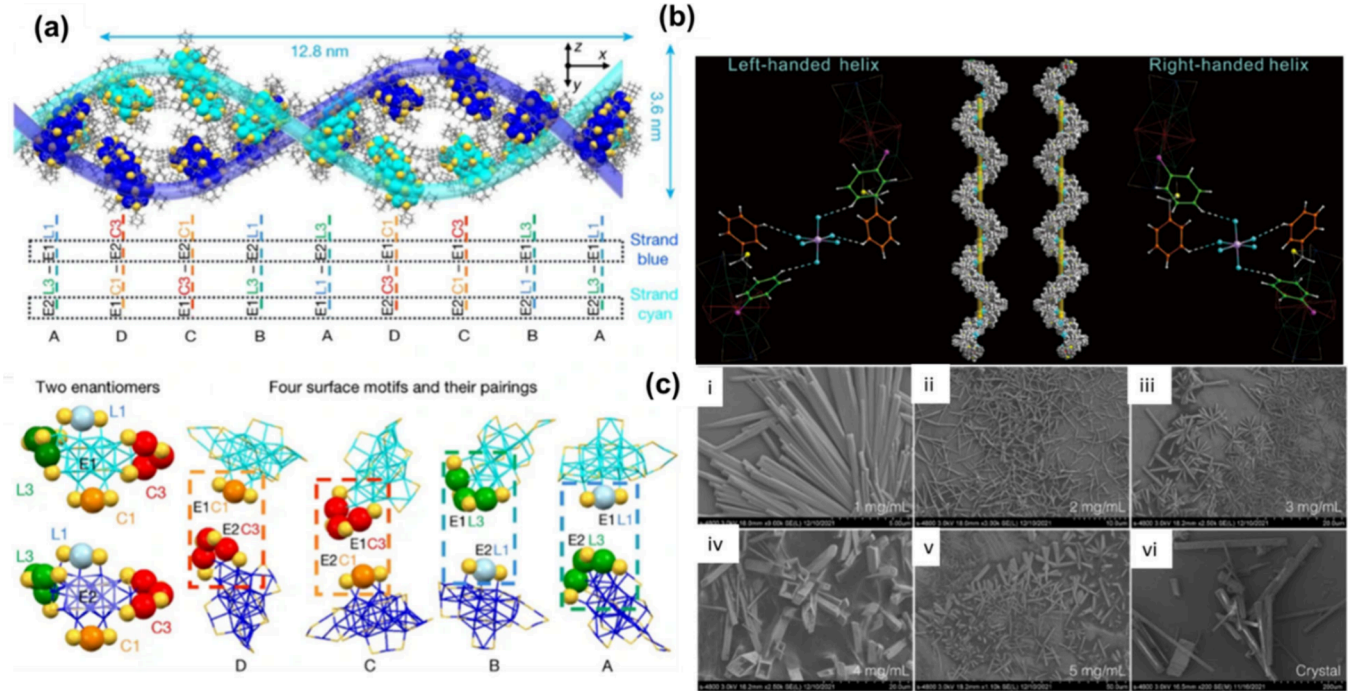

Figure 15. (a) Illustrations of the double-helical assembly of $Au_{29}(SAdm)_{19}$ NCs in supercrystals (top). Blue/cyan, Au; yellow, S; gray, C; white, H. The structures of two enantiomers are shown in the bottom left. The four surface motifs are represented by L1, L3, C1, and C3. L1 denotes the monomeric staple motif that has a shape similar to that of $Au_{30}(SAdm)_{18}$. L3 denotes the trimeric staple motif that has a shape similar to that of $Au_{30}(SAdm)_{18}$. C1 denotes the monomeric staple motif that has a shape similar to that of $Au_{28}(SC_6H_{11})_{20}$. C3 denotes the trimeric staple motif that has a shape similar to that of $Au_{28}(SC_6H_{11})_{20}$. Four different kinds of pairing between surface motifs are shown in the bottom right and in the middle. Reprinted with permission from ref 120. Copyright (2021) Springer Nature. (b) Left and right panels show diagrams along the axis of helices with intermolecular CH···F hydrogen bonds between the phenol groups, naphthalene groups, and $[SbF_6]^-$. In the middle, the diagram shows the structure of left- and right-handed helices. Red, Au; green, Ag; blue, Cu; pink, P; yellow, S; lavender, Sb; turquoise, F; gray, bright green and orange, C; white, H. Reprinted with permission from ref 121. Copyright (2021) Wiley. (c) SEM images after the volatilization of cluster solutions with different concentrations: (i) 1 mg/mL, (ii) 2 mg/mL, (iii) 3 mg/mL, (iv) 4 mg/mL, (v) 5 mg/mL, and (vi) crystal. Reprinted with permission from ref 122. Copyright (2022) American Chemical Society.

https://doi.org/10.1021/prechem.4c00044
Precis. Chem. 2024, 2, 495−517

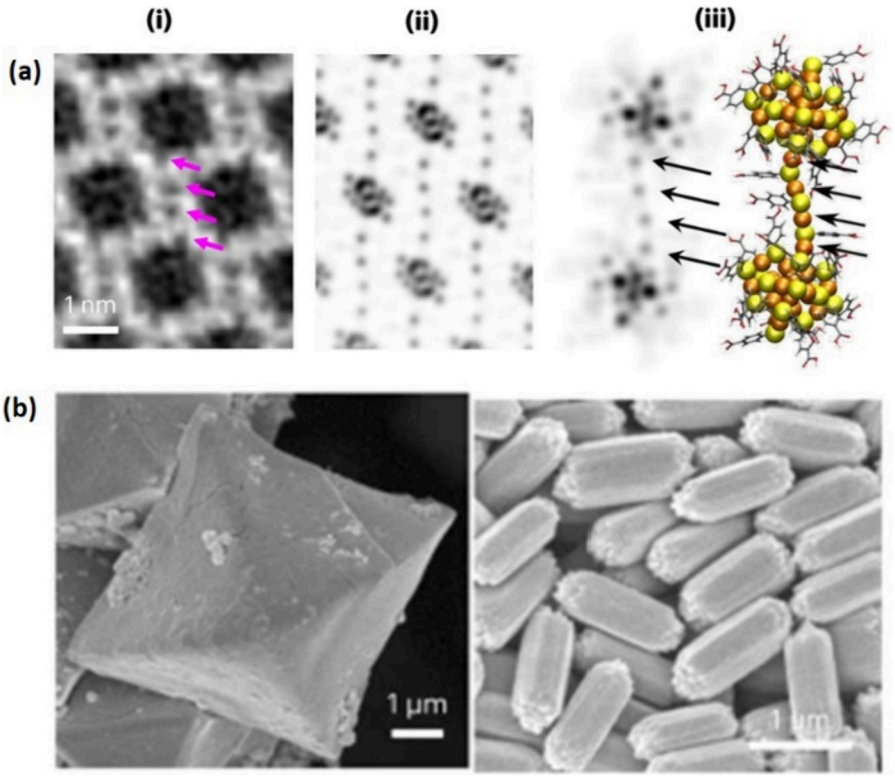

Figure 16. (a) NC packing structures of hexagonal rod-like supercrystals: (i) magnified bright-field ultralow-dose TEM image of supercrystal packing, (ii) simulated TEM image, and (iii) comparison between simulated TEM image (left) and atomic arrangement model (right) of the two $[Au_{25}(p\text{-MBA})_{18}]^-$ linked through the SR-[Au(I)-SR]$_4$. Orange, Au; yellow, S. (b) A field emission scanning electron microscopy (FESEM) image of octahedral self-assembly structure (left) and hexagonal rod-like self-assembly structure (right). Panels a and b are reprinted with permission from ref 54. Copyright (2023) Springer Nature.

double-helical DNA structure, and the double helix almost became an exclusive name for DNA. Similar structures can be found in the self-assembly of Au NCs.[120] In Figure 15a, $Au_{29}(SAdm)_{19}$ was synthesized and assembled into double or quadruple helixes (SAdm denotes adamantanethiolate) by Jin and co-workers. Such assembly was made possible by the interplay of van der Waals forces and steric hindrance due to the pairing of the motifs. These motif-matching interactions had interesting similarities with the base-pairing interaction of DNA. Zheng and co-workers utilized CH···π interaction and directed the growth of a chiral single helix (Figure 15b).[121] Similarly, a triple helix by gold−copper alloy NCs utilizing strong intermolecular interactions, such as $\pi\cdots\pi$ stacking and hydrogen bonding, was synthesized by Zhu and co-workers (Figure 15c).[122] With increasing publication volume about the self-assembly behavior of NCs, it is expected that the complex formation mechanism and structures can be further explained and predicted with more quantifiable interaction parameters.

5.2. Adjustable Assembly Morphology for Hydrophilic NCs

Reports on the crystallization of hydrophilic metal NCs are rare in comparison to those of the hydrophobic metal NCs discussed in the above section. Consequentially, these aqueous NCs have not been well studied by single crystal X-ray diffraction (SC-XRD). Atomic precision is seldom reached in the structure characterization of hydrophilic metal NCs, leaving alone quantitative studying of their structure−property relationship. This difficulty may arise from the complex aqueous environment, such as the changes in pH values and the presence of impurities in the crystallization solution, or the flexibility of most hydrophilic ligands.[123] On the other hand, this variability in solvent conditions may be fine-tuned to obtain a variety of self-assembled structures. Hence, many studies of hydrophilic NCs' self-assembly emphasize the manipulation of assembly's morphology through altering solvent conditions or addition of assisting ions.[118,119]

Delicate control of the self-assembly morphology is achieved for $Au_{102}(p\text{-MBA})_{44}$. As the *p*-MBA ligands are not located uniformly on the surface of NCs, more carboxylate groups are present at the equatorial position of the oval-shaped NCs. Hence, hydrogen bonding between equatorial carboxylate groups helped the formation of 2-dimensional nanosheet. By the addition of methanol, packing defects on the nanosheet occurred possibly due to the disrupted intercluster hydrogen bonding. These defects induced the curvature of assembly structure and resulted in the shape of a closed shell.[111] Another strategy for adjusting the self-assembly of hydrophilic NCs was to promoting surface dynamics of metal NCs by the addition of selected structure-directing agents.[54,124] In a recent work by Yao et al.,[54] morphology control over the resulting assembly was achieved for $Au_{25}(p\text{-MBA})_{18}$, as shown in Figure 16a. The closeness between simulated TEM images with the actual one provided strong support for the presence of SR-[Au(I)-SR]$_4$ interparticle linkers. Evidence such as 2D ^{1}H−^{1}H nuclear Overhauser effect spectroscopy (NOESY) and molecular dynamics simulation showed the importance of CH···π interaction between the linker and the counterion, tetraalkylammonium (TEA^+). Hexagonal rod-like supercrystals were sustained and stabilized by the interaction, while the absence of TEA^+ resulted in fcc (face-centered-cubic) octahedral supercrystals (Figure 16b). Hence, TEA^+ as structure-directing

https://doi.org/10.1021/prechem.4c00044
Precis. Chem. 2024, 2, 495−517

agent may interact or stabilize dynamically dissociated SR-[Au-SR]$_2$motifs on the surface of NCs, facilitating their further conjugation with adjacent NCs to form 1D nanowires. Close packing of such 1D nanowires gives rise to rod-like supercrystals. For hydrophilic NCs, the complexity in solvent conditions leads to both challenges in atomical resolution and a variety of structures.

6. CONCLUSION AND PERSPECTIVES

In summary, we have focused our attention on the molecular interactions of metal NCs at the nanoscale. We have discussed the role of intermolecular and intramolecular interactions as well as the interactions of these NCs with their specific solvent environment and small molecules. The discussion progresses from NCs' inner metal core through the ligand shell to the external assembly. For the metal core, surface forces, including intracluster ligand interaction, or interaction with solvent molecules or cations, are found effective in fine-tuning the structure and Au−Au distance. After the discussion of the metal core, we decipher many works on ligand shell engineering which facilitate property manipulation of metal NCs. First, to power up the PL of NCs, restricting the intramolecular motion through surface engineering is often adopted, although there are many environmental factors affecting the PLQY of NCs, such as the presence of oxygen or the state of aggregation. Second, for enhancing the catalytic performance of NCs, making room among ligand shells to increase the accessibility of active sites is often necessary, though engineering the electronic structure for better adsorption of small reactant molecules is also important. Finally, the self-assembly behavior of hydrophilic and hydrophobic NCs is investigated to understand phenomena such as the bulkiness of the motif layer, the interdigitation of ligands, and the structural distortion/dynamics.

This review also proposes several recommendations for deepening the understanding of NC interactions at the nanoscale. To start with, atomically precise NCs present a great opportunity for accurately pinpointing the cause of structural distortion for nanomaterials. Unlike nanoparticles, which are often approximated as spheres or rods, metal NCs can be studied in detail, down to the atomic level. Hence, in order to broaden our knowledge of atomic precision, data from cutting-edge characterization methodologies and analytical instruments for NCs should be better handled and analyzed. For example, atomic packing modes in the metal core can be probed by various X-ray techniques or TEM. Nuclear magnetic resonance (NMR) spectroscopy is one of the ways to investigate the interaction between molecules. Besides density functional theory (DFT) calculation, computational techniques such as molecular dynamics help to capture the surface dynamics of NCs. However, caution may be taken for two main problems. First, the experimental evidence on the structural detail of hydrophilic NCs is much less compared to that of their hydrophobic counterpart. Second, the resolved NC structure is often in the crystalline state, which does not account for motif dynamics or structural changes in the dissolved state.[26,27] Hence, with a wider application of spectroscopic techniques, more unknown NC structures are expected to be worked out, and atomic-detailed pictures of nanoscale molecular interaction will replace the inaccurate ones.

Furthermore, with increasing knowledge about the interaction between NCs and their environment, we can design our NCs as building blocks for responsive molecular devices that can perform specific functions in response to external stimuli.[125−128] Nanosensors for sensing pH change or the presence of certain ions are common subjects of investigation.[129−134]

Lastly, despite having many reports on the above-mentioned topics, such as the PL or catalysis of the metal NCs, there is a lack of systematic investigation into the interplay between molecular forces and the NCs. It is difficult to draw generalized conclusions or establish universal principles that govern NC behavior. One primary challenge is the complexity and diversity of NC systems. As highlighted throughout this review, each example of NC interaction or assembly presents a unique case, often involving multiple factors, such as various ligand functional groups, different metal core compositions or structures, and complicated environmental conditions. For instance, the interactions between NCs and their supports in catalytic systems have seldom been studied. Moreover, the structure of NCs as catalysts can be very dynamic, with rapid changes occurring during the catalytic process. These dynamic processes frequently elude investigation with current experimental techniques. The second challenge concerns the purity of the NCs. Despite the discovery of numerous NC species, not all receive a thorough investigation or subsequent utilization in different applications. This is often due to difficulties in achieving high purity and quantity after synthesis or purification. There is a pressing need to improve synthesis and isolation techniques, so that any possible impurity effects can be fairly ruled out in cluster research. The third difficulty is due to the multiscale nature of interactions. NCs exhibit behaviors that span multiple length scales, from atomic-level interactions within the core to mesoscale assembly processes. Bridging these different scales remains a significant challenge.

We hope that this review can inspire more fundamental and applied research in the field of NCs and/or nanoparticles. It is expected that areas such as the rational design of functional nanomaterials and precise control of nanochemistry processes could greatly benefit from quantitative investigations into NC interactions.

AUTHOR INFORMATION

Corresponding Authors

Qiaofeng Yao − *Key Laboratory of Organic Integrated Circuits, Ministry of Education & Tianjin Key Laboratory of Molecular Optoelectronic Sciences, Department of Chemistry, School of Science, Tianjin University, Tianjin 300072, P.R. China; Collaborative Innovation Center of Chemical Science and Engineering (Tianjin), Tianjin 300072, P.R. China;* orcid.org/0000-0002-5129-9343; Email: qfyao@tju.edu.cn

Jianping Xie − *Joint School of National University of Singapore and Tianjin University, International Campus of Tianjin University, Fuzhou 350207, P.R. China; Department of Chemical and Biomolecular Engineering, National University of Singapore, Singapore 117585, Singapore;* orcid.org/0000-0002-3254-5799; Email: chexiej@nus.edu.sg

Authors

Jing Qian − *Joint School of National University of Singapore and Tianjin University, International Campus of Tianjin University, Fuzhou 350207, P.R. China; Department of*

https://doi.org/10.1021/prechem.4c00044
Precis. Chem. 2024, 2, 495−517

Chemical and Biomolecular Engineering, National University of Singapore, Singapore 117585, Singapore

Zhucheng Yang − *Joint School of National University of Singapore and Tianjin University, International Campus of Tianjin University, Fuzhou 350207, P.R. China; Department of Chemical and Biomolecular Engineering, National University of Singapore, Singapore 117585, Singapore*

Jingkuan Lyu − *Joint School of National University of Singapore and Tianjin University, International Campus of Tianjin University, Fuzhou 350207, P.R. China; Department of Chemical and Biomolecular Engineering, National University of Singapore, Singapore 117585, Singapore*

Complete contact information is available at: https://pubs.acs.org/10.1021/prechem.4c00044

Notes

The authors declare no competing financial interest.

■ ACKNOWLEDGMENTS

We acknowledge the financial support from National Natural Science Foundation of China (22071174, 22371204) and Ministry of Education, Singapore (grant no. A-8000054-01-00). Q. Yao acknowledges the financial support from Fundamental Research Funds for the Central Universities.

■ REFERENCES

(1) Bishop, K. J. M.; Wilmer, C. E.; Soh, S.; Grzybowski, B. A. Nanoscale Forces and Their Uses in Self-Assembly. *Small* **2009**, *5* (14), 1600−1630.

(2) Nel, A. E.; Mädler, L.; Velegol, D.; Xia, T.; Hoek, E. M. V.; Somasundaran, P.; Klaessig, F.; Castranova, V.; Thompson, M. Understanding Biophysicochemical Interactions at the Nano−Bio Interface. *Nat. Mater.* **2009**, *8* (7), 543−557.

(3) Min, Y.; Akbulut, M.; Kristiansen, K.; Golan, Y.; Israelachvili, J. The Role of Interparticle and External Forces in Nanoparticle Assembly. *Nat. Mater.* **2008**, *7* (7), 527−538.

(4) Chakraborty, I.; Pradeep, T. Atomically Precise Clusters of Noble Metals: Emerging Link between Atoms and Nanoparticles. *Chem. Rev.* **2017**, *117* (12), 8208−8271.

(5) Jin, R.; Zeng, C.; Zhou, M.; Chen, Y. Atomically Precise Colloidal Metal Nanoclusters and Nanoparticles: Fundamentals and Opportunities. *Chem. Rev.* **2016**, *116* (18), 10346−10413.

(6) Yao, Q.; Yuan, X.; Chen, T.; Leong, D. T.; Xie, J. Engineering Functional Metal Materials at the Atomic Level. *Adv. Mater.* **2018**, *30* (47), 1802751.

(7) Lu, Y.; Chen, W. Sub-Nanometre Sized Metal Clusters: From Synthetic Challenges to the Unique Property Discoveries. *Chem. Soc. Rev.* **2012**, *41* (9), 3594−3623.

(8) Zeng, C.; Chen, Y.; Kirschbaum, K.; Lambright, K. J.; Jin, R. Emergence of Hierarchical Structural Complexities in Nanoparticles and Their Assembly. *Science* **2016**, *354* (6319), 1580−1584.

(9) Fernando, A.; Weerawardene, K. L. D. M.; Karimova, N. V.; Aikens, C. M. Quantum Mechanical Studies of Large Metal, Metal Oxide, and Metal Chalcogenide Nanoparticles and Clusters. *Chem. Rev.* **2015**, *115* (12), 6112−6216.

(10) Wu, Z.; Yao, Q.; Chai, O. J. H.; Ding, N.; Xu, W.; Zang, S.; Xie, J. Unraveling the Impact of Gold(I)−Thiolate Motifs on the Aggregation-Induced Emission of Gold Nanoclusters. *Angew. Chem.* **2020**, *132* (25), 10020−10025.

(11) Shang, L.; Dong, S.; Nienhaus, G. U. Ultra-Small Fluorescent Metal Nanoclusters: Synthesis and Biological Applications. *Nano Today* **2011**, *6* (4), 401−418.

(12) Luo, Z.; Yuan, X.; Yu, Y.; Zhang, Q.; Leong, D. T.; Lee, J. Y.; Xie, J. From Aggregation-Induced Emission of Au(I)−Thiolate Complexes to Ultrabright Au(0)@Au(I)−Thiolate Core−Shell Nanoclusters. *J. Am. Chem. Soc.* **2012**, *134* (40), 16662−16670.

(13) Goswami, N.; Yao, Q.; Luo, Z.; Li, J.; Chen, T.; Xie, J. Luminescent Metal Nanoclusters with Aggregation-Induced Emission. *J. Phys. Chem. Lett.* **2016**, *7* (6), 962−975.

(14) Knoppe, S.; Bürgi, T. Chirality in Thiolate-Protected Gold Clusters. *Acc. Chem. Res.* **2014**, *47* (4), 1318−1326.

(15) Zhu, M.; Aikens, C. M.; Hendrich, M. P.; Gupta, R.; Qian, H.; Schatz, G. C.; Jin, R. Reversible Switching of Magnetism in Thiolate-Protected Au_{25} Superatoms. *J. Am. Chem. Soc.* **2009**, *131* (7), 2490−2492.

(16) Li, Y.; Jin, R. Magnetism of Atomically Precise Gold and Doped Nanoclusters: Delocalized Spin and Interparticle Coupling. *J. Phys. Chem. C* **2021**, *125* (29), 15773−15784.

(17) Fang, J.; Zhang, B.; Yao, Q.; Yang, Y.; Xie, J.; Yan, N. Recent Advances in the Synthesis and Catalytic Applications of Ligand-Protected, Atomically Precise Metal Nanoclusters. *Coord. Chem. Rev.* **2016**, *322*, 1−29.

(18) Yamazoe, S.; Koyasu, K.; Tsukuda, T. Nonscalable Oxidation Catalysis of Gold Clusters. *Acc. Chem. Res.* **2014**, *47* (3), 816−824.

(19) Pyo, K.; Thanthirige, V. D.; Kwak, K.; Pandurangan, P.; Ramakrishna, G.; Lee, D. Ultrabright Luminescence from Gold Nanoclusters: Rigidifying the Au(I)−Thiolate Shell. *J. Am. Chem. Soc.* **2015**, *137* (25), 8244−8250.

(20) Shi, W.-Q.; Zeng, L.; He, R.-L.; Han, X.-S.; Guan, Z.-J.; Zhou, M.; Wang, Q.-M. Near-Unity NIR Phosphorescent Quantum Yield from a Room-Temperature Solvated Metal Nanocluster. *Science* **2024**, *383* (6680), 326−330.

(21) Zeng, C.; Chen, Y.; Das, A.; Jin, R. Transformation Chemistry of Gold Nanoclusters: From One Stable Size to Another. *J. Phys. Chem. Lett.* **2015**, *6* (15), 2976−2986.

(22) Chen, Y.; Zeng, C.; Kauffman, D. R.; Jin, R. Tuning the Magic Size of Atomically Precise Gold Nanoclusters via Isomeric Methylbenzenethiols. *Nano Lett.* **2015**, *15* (5), 3603−3609.

(23) Chen, Y.; Zeng, C.; Liu, C.; Kirschbaum, K.; Gayathri, C.; Gil, R. R.; Rosi, N. L.; Jin, R. Crystal Structure of Barrel-Shaped Chiral Au_{130}(p-MBT)$_{50}$ Nanocluster. *J. Am. Chem. Soc.* **2015**, *137* (32), 10076−10079.

(24) Tang, Q.; Ouyang, R.; Tian, Z.; Jiang, D. The Ligand Effect on the Isomer Stability of $Au_{24}(SR)_{20}$ Clusters. *Nanoscale* **2015**, *7* (6), 2225−2229.

(25) Chen, Y.; Liu, C.; Tang, Q.; Zeng, C.; Higaki, T.; Das, A.; Jiang, D.; Rosi, N. L.; Jin, R. Isomerism in $Au_{28}(SR)_{20}$ Nanocluster and Stable Structures. *J. Am. Chem. Soc.* **2016**, *138* (5), 1482−1485.

(26) Chevrier, D. M.; Raich, L.; Rovira, C.; Das, A.; Luo, Z.; Yao, Q.; Chatt, A.; Xie, J.; Jin, R.; Akola, J.; Zhang, P. Molecular-Scale Ligand Effects in Small Gold−Thiolate Nanoclusters. *J. Am. Chem. Soc.* **2018**, *140* (45), 15430−15436.

(27) Chevrier, D. M.; Conn, B. E.; Li, B.; Jiang, D.; Bigioni, T. P.; Chatt, A.; Zhang, P. Interactions between Ultrastable $Na_4Ag_{44}(SR)_{30}$ Nanoclusters and Coordinating Solvents: Uncovering the Atomic-Scale Mechanism. *ACS Nano* **2020**, *14* (7), 8433−8441.

(28) MacDonald, M. A.; Chevrier, D. M.; Zhang, P.; Qian, H.; Jin, R. The Structure and Bonding of $Au_{25}(SR)_{18}$ Nanoclusters from EXAFS: The Interplay of Metallic and Molecular Behavior. *J. Phys. Chem. C* **2011**, *115* (31), 15282−15287.

(29) Matus, M. F.; Malola, S.; Kinder Bonilla, E.; Barngrover, B. M.; Aikens, C. M.; Häkkinen, H. A Topological Isomer of the $Au_{25}(SR)_{18}^-$ Nanocluster. *Chem. Commun.* **2020**, *56* (58), 8087−8090.

(30) Cao, Y.; Malola, S.; Matus, M. F.; Chen, T.; Yao, Q.; Shi, R.; Häkkinen, H.; Xie, J. Reversible Isomerization of Metal Nanoclusters Induced by Intermolecular Interaction. *Chem.* **2021**, *7* (8), 2227−2244.

(31) Gan, Z.; Liu, Y.; Wang, L.; Jiang, S.; Xia, N.; Yan, Z.; Wu, X.; Zhang, J.; Gu, W.; He, L.; Dong, J.; Ma, X.; Kim, J.; Wu, Z.; Xu, Y.; Li, Y.; Wu, Z. Distance Makes a Difference in Crystalline Photoluminescence. *Nat. Commun.* **2020**, *11* (1), 5572.

(32) Gan, Z.; Chen, J.; Liao, L.; Zhang, H.; Wu, Z. Surface Single-Atom Tailoring of a Gold Nanoparticle. *J. Phys. Chem. Lett.* **2018**, *9* (1), 204−208.

(33) Zhou, Y.; Liao, L.; Zhuang, S.; Zhao, Y.; Gan, Z.; Gu, W.; Li, J.; Deng, H.; Xia, N.; Wu, Z. Traceless Removal of Two Kernel Atoms in a Gold Nanocluster and Its Impact on Photoluminescence. *Angew. Chem., Int. Ed.* **2021**, *60* (16), 8668−8672.
(34) Wang, S.; Meng, X.; Das, A.; Li, T.; Song, Y.; Cao, T.; Zhu, X.; Zhu, M.; Jin, R. A 200-Fold Quantum Yield Boost in the Photoluminescence of Silver-Doped Ag_xAu_{25-x} Nanoclusters: The 13 Th Silver Atom Matters. *Angew. Chem., Int. Ed.* **2014**, *53* (9), 2376−2380.
(35) Yu, Y.; Luo, Z.; Chevrier, D. M.; Leong, D. T.; Zhang, P.; Jiang, D.; Xie, J. Identification of a Highly Luminescent $Au_{22}(SG)_{18}$ Nanocluster. *J. Am. Chem. Soc.* **2014**, *136* (4), 1246−1249.
(36) Luo, Z.; Nachammai, V.; Zhang, B.; Yan, N.; Leong, D. T.; Jiang, D.; Xie, J. Toward Understanding the Growth Mechanism: Tracing All Stable Intermediate Species from Reduction of Au(I)−Thiolate Complexes to Evolution of Au_{25} Nanoclusters. *J. Am. Chem. Soc.* **2014**, *136* (30), 10577−10580.
(37) Deng, H.-H.; Shi, X.-Q.; Wang, F.-F.; Peng, H.-P.; Liu, A.-L.; Xia, X.-H.; Chen, W. Fabrication of Water-Soluble, Green-Emitting Gold Nanoclusters with a 65% Photoluminescence Quantum Yield via Host−Guest Recognition. *Chem. Mater.* **2017**, *29* (3), 1362−1369.
(38) Zhong, Y.; Zhang, J.; Li, T.; Xu, W.; Yao, Q.; Lu, M.; Bai, X.; Wu, Z.; Xie, J.; Zhang, Y. Suppression of Kernel Vibrations by Layer-by-Layer Ligand Engineering Boosts Photoluminescence Efficiency of Gold Nanoclusters. *Nat. Commun.* **2023**, *14* (1), 658.
(39) Wei, S.; Li, Z.; Lu, W.; Liu, H.; Zhang, J.; Chen, T.; Tang, B. Z. Multicolor Fluorescent Polymeric Hydrogels. *Angew. Chem., Int. Ed.* **2021**, *60* (16), 8608−8624.
(40) Rashi; Bain, D.; Devi, A.; Chakraborty, S.; Patra, A. Cationic Polymer Functionalized Copper Nanocluster-Based Fluorescent Probe for the Selective and Sensitive Detection of S^{2-} Ions. *ACS Sustainable Chem. Eng.* **2023**, *11* (5), 1995−2004.
(41) Casteleiro, B.; Da Cruz-Boisson, F.; Alcouffe, P.; Pinto, S. N.; Gaspar Martinho, J. M.; Charreyre, M.-T.; Farinha, J. P. S.; Favier, A. Near-Infrared-Luminescent Gold Nanoclusters Stabilized by End-Grafted Biocompatible Polymer Chains for Bioimaging. *ACS Appl. Nano Mater.* **2023**, *6* (13), 11689−11698.
(42) Hao, N.; Cao, Y.; Li, R.; Lin, H.; Shan, H.; Chen, T.; Chai, O. J. H.; Yao, Q.; Chen, X.; Xie, J. Cation Polymer-Induced Aggregation of Water-Soluble Au(I)-Thiolate Complexes and Their Photoluminescence Properties. *Chem. Commun.* **2022**, *58* (59), 8234−8237.
(43) Goswami, N.; Lin, F.; Liu, Y.; Leong, D. T.; Xie, J. Highly Luminescent Thiolated Gold Nanoclusters Impregnated in Nanogel. *Chem. Mater.* **2016**, *28* (11), 4009−4016.
(44) Deng, H.; Huang, K.; Xiu, L.; Sun, W.; Yao, Q.; Fang, X.; Huang, X.; Noreldeen, H. A. A.; Peng, H.; Xie, J.; Chen, W. Bis-Schiff Base Linkage-Triggered Highly Bright Luminescence of Gold Nanoclusters in Aqueous Solution at the Single-Cluster Level. *Nat. Commun.* **2022**, *13* (1), 3381.
(45) Pyo, K.; Ly, N. H.; Yoon, S. Y.; Shen, Y.; Choi, S. Y.; Lee, S. Y.; Joo, S.-W.; Lee, D. Highly Luminescent Folate-Functionalized Au_{22} Nanoclusters for Bioimaging. *Adv. Healthc. Mater.* **2017**, *6* (16), 1700203.
(46) Pyo, K.; Thanthirige, V. D.; Yoon, S. Y.; Ramakrishna, G.; Lee, D. Enhanced Luminescence of $Au_{22}(SG)_{18}$ Nanoclusters via Rational Surface Engineering. *Nanoscale* **2016**, *8* (48), 20008−20016.
(47) Kang, X.; Zhu, M. Tailoring the Photoluminescence of Atomically Precise Nanoclusters. *Chem. Soc. Rev.* **2019**, *48* (8), 2422−2457.
(48) Bonacchi, S.; Cantelli, A.; Battistelli, G.; Guidetti, G.; Calvaresi, M.; Manzi, J.; Gabrielli, L.; Ramadori, F.; Gambarin, A.; Mancin, F.; Montalti, M. Photoswitchable NIR-Emitting Gold Nanoparticles. *Angew. Chem., Int. Ed.* **2016**, *55* (37), 11064−11068.
(49) Rival, J. V.; Mymoona, P.; Lakshmi, K. M.; Pradeep, T.; Shibu, E. S.; et al. Self-Assembly of Precision Noble Metal Nanoclusters: Hierarchical Structural Complexity, Colloidal Superstructures, and Applications. *Small* **2021**, *17* (27), 2005718.
(50) Shi, L.; Zhu, L.; Guo, J.; Zhang, L.; Shi, Y.; Zhang, Y.; Hou, K.; Zheng, Y.; Zhu, Y.; Lv, J.; Liu, S.; Tang, Z. Self-Assembly of Chiral Gold Clusters into Crystalline Nanocubes of Exceptional Optical Activity. *Angew. Chem., Int. Ed.* **2017**, *56* (48), 15397−15401.
(51) Wu, Z.; Du, Y.; Liu, J.; Yao, Q.; Chen, T.; Cao, Y.; Zhang, H.; Xie, J. Aurophilic Interactions in the Self-Assembly of Gold Nanoclusters into Nanoribbons with Enhanced Luminescence. *Angew. Chem., Int. Ed.* **2019**, *58* (24), 8139−8144.
(52) Qian, L.; Tong, B.; Shen, J.; Shi, J.; Zhi, J.; Dong, Y.; Yang, F.; Dong, Y.; Lam, J. W. Y.; Liu, Y.; Tang, B. Z. Crystallization-Induced Emission Enhancement in a Phosphorus-Containing Heterocyclic Luminogen. *J. Phys. Chem. B* **2009**, *113* (27), 9098−9103.
(53) Yin, Z.; Wang, Z.; Dai, X.; Liu, N.; Wang, S.; Li, G.; Du, F.; Yuan, X. Highly Luminescent AuAg Nanoclusters with Aggregation-Induced Emission for High-Performance White LED Application. *ACS Sustain. Chem. Eng.* **2020**, *8* (40), 15336−15343.
(54) Yao, Q.; Liu, L.; Malola, S.; Ge, M.; Xu, H.; Wu, Z.; Chen, T.; Cao, Y.; Matus, M. F.; Pihlajamäki, A.; Han, Y.; Häkkinen, H.; Xie, J. Supercrystal Engineering of Atomically Precise Gold Nanoparticles Promoted by Surface Dynamics. *Nat. Chem.* **2023**, *15*, 230.
(55) Chen, T.; Yang, S.; Chai, J.; Song, Y.; Fan, J.; Rao, B.; Sheng, H.; Yu, H.; Zhu, M. Crystallization-Induced Emission Enhancement: A Novel Fluorescent Au-Ag Bimetallic Nanocluster with Precise Atomic Structure. *Sci. Adv.* **2017**, *3* (8), No. e1700956.
(56) Yao, C.; Xu, C.; Park, I.; Zhao, M.; Zhu, Z.; Li, J.; Hai, X.; Fang, H.; Zhang, Y.; Macam, G.; Teng, J.; Li, L.; Xu, Q.; Chuang, F.; Lu, J.; Su, C.; Li, J.; Lu, J. Giant Emission Enhancement of Solid-State Gold Nanoclusters by Surface Engineering. *Angew. Chem., Int. Ed.* **2020**, *59* (21), 8270−8276.
(57) Si, W.-D.; Sheng, K.; Zhang, C.; Wang, Z.; Zhang, S.-S.; Dou, J.-M.; Feng, L.; Gao, Z.-Y.; Tung, C.-H.; Sun, D. Bicarbonate Insertion Triggered Self-Assembly of Chiral Octa-Gold Nanoclusters into Helical Superstructures in the Crystalline State. *Chem. Sci.* **2022**, *13* (35), 10523−10531.
(58) Bi, Y.; Wang, Z.; Liu, T.; Sun, D.; Godbert, N.; Li, H.; Hao, J.; Xin, X. Supramolecular Chirality from Hierarchical Self-Assembly of Atomically Precise Silver Nanoclusters Induced by Secondary Metal Coordination. *ACS Nano* **2021**, *15* (10), 15910−15919.
(59) Xie, Z.; Sun, P.; Wang, Z.; Li, H.; Yu, L.; Sun, D.; Chen, M.; Bi, Y.; Xin, X.; Hao, J. Metal−Organic Gels from Silver Nanoclusters with Aggregation-Induced Emission and Fluorescence-to-Phosphorescence Switching. *Angew. Chem. Int. Ed* **2020**, *59* (25), 9922−9927.
(60) Feng, N.; Wang, Z.; Sun, D.; Sun, P.; Xin, X.; Cheng, X.; Li, H. Circularly Polarized Phosphorescence from Cocrystallization of Atomic Precise Silver Nanoclusters with Tartaric Acid. *Advanced Optical Materials* **2022**, *10* (15), 2102319.
(61) Wan, Q.; Yang, J.; To, W.-P.; Che, C.-M. Strong Metal−Metal Pauli Repulsion Leads to Repulsive Metallophilicity in Closed-Shell d^8 and d^{10} Organometallic Complexes. *Proc. Natl. Acad. Sci. U. S. A.* **2021**, *118* (1), No. e2019265118.
(62) Yao, L.-Y.; Yam, V. W.-W. Dual Emissive Gold(I)−Sulfido Cluster Framework Capable of Benzene−Cyclohexane Separation in the Solid State Accompanied by Luminescence Color Changes. *J. Am. Chem. Soc.* **2021**, *143* (6), 2558−2566.
(63) Yan, L.-L.; Yao, L.-Y.; Ng, M.; Tang, W. K.; Leung, M.-Y.; Yam, V. W.-W. Stimuli-Induced Reversible Transformation between Decanuclear and Pentanuclear Gold(I) Sulfido Complexes. *J. Am. Chem. Soc.* **2022**, *144* (43), 19748−19757.
(64) Han, Z.; Zhao, X.; Peng, P.; Li, S.; Zhang, C.; Cao, M.; Li, K.; Wang, Z.-Y.; Zang, S.-Q. Intercluster Aurophilicity-Driven Aggregation Lighting Circularly Polarized Luminescence of Chiral Gold Clusters. *Nano Res.* **2020**, *13* (12), 3248−3252.
(65) Li, H.; Kang, X.; Zhu, M. Controlling the Nature of Photoluminescence of Emissive Metal Nanoclusters. *ChemPhysChem* **2022**, *23* (23), No. e202200484.
(66) Yu, J.; Hu, D.; Barbara, P. F. Unmasking Electronic Energy Transfer of Conjugated Polymers by Suppression of O_2 Quenching. *Science* **2000**, *289* (5483), 1327−1330.
(67) Zhu, C.; Xin, J.; Li, J.; Li, H.; Kang, X.; Pei, Y.; Zhu, M. Fluorescence or Phosphorescence? The Metallic Composition of the

Nanocluster Kernel Does Matter. *Angew. Chem., Int. Ed.* **2022**, *61* (31). DOI: 10.1002/anie.202205947.
(68) Song, Y.; Li, Y.; Zhou, M.; Liu, X.; Li, H.; Wang, H.; Shen, Y.; Zhu, M.; Jin, R. Ultrabright Au@Cu_{14} Nanoclusters: 71.3% Phosphorescence Quantum Yield in Non-Degassed Solution at Room Temperature. *Sci. Adv.* **2021**, *7* (2), No. eabd2091.
(69) Hirai, H.; Takano, S.; Nakashima, T.; Iwasa, T.; Taketsugu, T.; Tsukuda, T. Doping-Mediated Energy-Level Engineering of M@Au_{12} Superatoms (M = Pd, Pt, Rh, Ir) for Efficient Photoluminescence and Photocatalysis. *Angew. Chem., Int. Ed.* **2022**, *61* (36). DOI: 10.1002/anie.202207290.
(70) Huang, R.-W.; Wei, Y.-S.; Dong, X.-Y.; Wu, X.-H.; Du, C.-X.; Zang, S.-Q.; Mak, T. C. W. Hypersensitive Dual-Function Luminescence Switching of a Silver-Chalcogenolate Cluster-Based Metal−Organic Framework. *Nat. Chem.* **2017**, *9* (7), 689−697.
(71) Sugiuchi, M.; Maeba, J.; Okubo, N.; Iwamura, M.; Nozaki, K.; Konishi, K. Aggregation-Induced Fluorescence-to-Phosphorescence Switching of Molecular Gold Clusters. *J. Am. Chem. Soc.* **2017**, *139* (49), 17731−17734.
(72) Wu, Z.; Yao, Q.; Zang, S.; Xie, J. Aggregation-Induced Emission in Luminescent Metal Nanoclusters. *Natl. Sci. Rev.* **2021**, *8* (6), No. nwaa208.
(73) Yao, L.-Y.; Low, K.-H.; Yam, V. W.-W. A Gold Quartet Framework with Reversible Anisotropic Structural Transformation Accompanied by Luminescence Response. *Chem.* **2019**, *5* (9), 2418−2428.
(74) Haruta, M. When Gold Is Not Noble: Catalysis by Nanoparticles. *Chem. Rec.* **2003**, *3* (2), 75−87.
(75) Sun, K.; Kohyama, M.; Tanaka, S.; Takeda, S. Understanding of the Activity Difference between Nanogold and Bulk Gold by Relativistic Effects. *J. Energy Chem.* **2015**, *24* (4), 485−489.
(76) Lopez, N.; Nørskov, J. K. Catalytic CO Oxidation by a Gold Nanoparticle: A Density Functional Study. *J. Am. Chem. Soc.* **2002**, *124* (38), 11262−11263.
(77) Jin, R.; Li, G.; Sharma, S.; Li, Y.; Du, X. Toward Active-Site Tailoring in Heterogeneous Catalysis by Atomically Precise Metal Nanoclusters with Crystallographic Structures. *Chem. Rev.* **2021**, *121* (2), 567−648.
(78) Li, J.; Nasaruddin, R. R.; Feng, Y.; Yang, J.; Yan, N.; Xie, J. Tuning the Accessibility and Activity of $Au_{25}(SR)_{18}$ Nanocluster Catalysts through Ligand Engineering. *Chem. - Eur. J.* **2016**, *22* (42), 14816−14820.
(79) Narouz, M. R.; Osten, K. M.; Unsworth, P. J.; Man, R. W. Y.; Salorinne, K.; Takano, S.; Tomihara, R.; Kaappa, S.; Malola, S.; Dinh, C.-T.; Padmos, J. D.; Ayoo, K.; Garrett, P. J.; Nambo, M.; Horton, J. H.; Sargent, E. H.; Häkkinen, H.; Tsukuda, T.; Crudden, C. M. N-Heterocyclic Carbene-Functionalized Magic-Number Gold Nanoclusters. *Nat. Chem.* **2019**, *11* (5), 419−425.
(80) Nasaruddin, R. R.; Chen, T.; Li, J.; Goswami, N.; Zhang, J.; Yan, N.; Xie, J. Ligands Modulate Reaction Pathway in the Hydrogenation of 4-Nitrophenol Catalyzed by Gold Nanoclusters. *ChemCatChem.* **2018**, *10* (2), 395−402.
(81) Nørskov, J. K.; Studt, F.; Abild-Pedersen, F.; Bligaard, T. *Fundamental Concepts in Heterogeneous Catalysis*; Wiley: Hoboken, NJ, 2015.
(82) Zhang, Y.; Song, P.; Chen, T.; Liu, X.; Chen, T.; Wu, Z.; Wang, Y.; Xie, J.; Xu, W. Unique Size-Dependent Nanocatalysis Revealed at the Single Atomically Precise Gold Cluster Level. *Proc. Natl. Acad. Sci. U. S. A.* **2018**, *115* (42), 10588−10593.
(83) Li, S.; Du, X.; Liu, Z.; Li, Y.; Shao, Y.; Jin, R. Size Effects of Atomically Precise Gold Nanoclusters in Catalysis. *Precis. Chem.* **2023**, *1* (1), 14−28.
(84) Zhou, M.; Zeng, C.; Chen, Y.; Zhao, S.; Sfeir, M. Y.; Zhu, M.; Jin, R. Evolution from the Plasmon to Exciton State in Ligand-Protected Atomically Precise Gold Nanoparticles. *Nat. Commun.* **2016**, *7* (1), 13240.
(85) Li, G.; Jiang, D.; Kumar, S.; Chen, Y.; Jin, R. Size Dependence of Atomically Precise Gold Nanoclusters in Chemoselective Hydrogenation and Active Site Structure. *ACS Catal.* **2014**, *4* (8), 2463−2469.
(86) Wang, S.; Jin, S.; Yang, S.; Chen, S.; Song, Y.; Zhang, J.; Zhu, M. Total Structure Determination of Surface Doping $[Ag_{46}Au_{24}(SR)_{32}](BPh_4)_2$ Nanocluster and Its Structure-Related Catalytic Property. *Sci. Adv.* **2015**, *1* (7), No. e1500441.
(87) Yuan, S.-F.; Guan, Z.-J.; Wang, Q.-M. Identification of the Active Species in Bimetallic Cluster Catalyzed Hydrogenation. *J. Am. Chem. Soc.* **2022**, *144* (25), 11405−11412.
(88) Liu, Y.; Chai, X.; Cai, X.; Chen, M.; Jin, R.; Ding, W.; Zhu, Y. Central Doping of a Foreign Atom into the Silver Cluster for Catalytic Conversion of CO_2 toward C−C Bond Formation. *Angew. Chem., Int. Ed.* **2018**, *57* (31), 9775−9779.
(89) Kwak, K.; Choi, W.; Tang, Q.; Kim, M.; Lee, Y.; Jiang, D.; Lee, D. A Molecule-like $PtAu_{24}(SC_6H_{13})_{18}$ Nanocluster as an Electrocatalyst for Hydrogen Production. *Nat. Commun.* **2017**, *8* (1), 14723.
(90) Wan, X.-K.; Wang, J.-Q.; Nan, Z.-A.; Wang, Q.-M. Ligand Effects in Catalysis by Atomically Precise Gold Nanoclusters. *Sci. Adv.* **2017**, *3* (10), No. e1701823.
(91) Shan, H.; Shi, J.; Chen, T.; Cao, Y.; Yao, Q.; An, H.; Yang, Z.; Wu, Z.; Jiang, Z.; Xie, J. Modulating Catalytic Activity and Stability of Atomically Precise Gold Nanoclusters as Peroxidase Mimics via Ligand Engineering. *ACS Nano* **2023**, *17* (3), 2368−2377.
(92) Zhang, B.; Chen, J.; Cao, Y.; Chai, O. J. H.; Xie, J. Ligand Design in Ligand-Protected Gold Nanoclusters. *Small* **2021**, *17* (27), 2004381.
(93) Liu, C.; Abroshan, H.; Yan, C.; Li, G.; Haruta, M. One-Pot Synthesis of $Au_{11}(PPh_2Py)_7Br_3$ for the Highly Chemoselective Hydrogenation of Nitrobenzaldehyde. *ACS Catal.* **2016**, *6* (1), 92−99.
(94) Yoskamtorn, T.; Yamazoe, S.; Takahata, R.; Nishigaki, J.; Thivasasith, A.; Limtrakul, J.; Tsukuda, T. Thiolate-Mediated Selectivity Control in Aerobic Alcohol Oxidation by Porous Carbon-Supported Au_{25} Clusters. *ACS Catal.* **2014**, *4* (10), 3696−3700.
(95) Wang, H.; Liu, X.; Yang, W.; Mao, G.; Meng, Z.; Wu, Z.; Jiang, H.-L. Surface-Clean Au_{25} Nanoclusters in Modulated Microenvironment Enabled by Metal−Organic Frameworks for Enhanced Catalysis. *J. Am. Chem. Soc.* **2022**, *144* (48), 22008−22017.
(96) Dong, J.; Robinson, J. R.; Gao, Z.-H.; Wang, L.-S. Selective Semihydrogenation of Polarized Alkynes by a Gold Hydride Nanocluster. *J. Am. Chem. Soc.* **2022**, *144* (27), 12501−12509.
(97) Tian, S.; Li, Y.-Z.; Li, M.-B.; Yuan, J.; Yang, J.; Wu, Z.; Jin, R. Structural Isomerism in Gold Nanoparticles Revealed by X-Ray Crystallography. *Nat. Commun.* **2015**, *6* (1), 8667.
(98) Good, J.; Duchesne, P. N.; Zhang, P.; Koshut, W.; Zhou, M.; Jin, R. On the Functional Role of the Cerium Oxide Support in the $Au_{38}(SR)_{24}/CeO_2$ Catalyst for CO Oxidation. *Catal. Today* **2017**, *280*, 239−245.
(99) Li, G.; Abroshan, H.; Chen, Y.; Jin, R.; Kim, H. J. Experimental and Mechanistic Understanding of Aldehyde Hydrogenation Using Au_{25} Nanoclusters with Lewis Acids: Unique Sites for Catalytic Reactions. *J. Am. Chem. Soc.* **2015**, *137* (45), 14295−14304.
(100) Abroshan, H.; Li, G.; Lin, J.; Kim, H. J.; Jin, R. Molecular Mechanism for the Activation of $Au_{25}(SCH_2CH_2Ph)_{18}$ Nanoclusters by Imidazolium-Based Ionic Liquids for Catalysis. *J. Catal.* **2016**, *337*, 72−79.
(101) Li, G.; Abroshan, H.; Liu, C.; Zhuo, S.; Li, Z.; Xie, Y.; Kim, H. J.; Rosi, N. L.; Jin, R. Tailoring the Electronic and Catalytic Properties of Au_{25} Nanoclusters *via* Ligand Engineering. *ACS Nano* **2016**, *10* (8), 7998−8005.
(102) Gao, Z.-H.; Wei, K.; Wu, T.; Dong, J.; Jiang, D.; Sun, S.; Wang, L.-S. A Heteroleptic Gold Hydride Nanocluster for Efficient and Selective Electrocatalytic Reduction of CO_2 to CO. *J. Am. Chem. Soc.* **2022**, *144* (12), 5258−5262.
(103) Yuan, S.; Lei, Z.; Guan, Z.; Wang, Q. Atomically Precise Preorganization of Open Metal Sites on Gold Nanoclusters with High Catalytic Performance. *Angew. Chem., Int. Ed.* **2021**, *60* (10), 5225−5229.

(104) Li, Y.; Kim, H. K.; McGillicuddy, R. D.; Zheng, S.-L.; Anderton, K. J.; Stec, G. J.; Lee, J.; Cui, D.; Mason, J. A. A Double Open-Shelled Au_{43} Nanocluster with Increased Catalytic Activity and Stability. *J. Am. Chem. Soc.* **2023**, *145* (16), 9304−9312.
(105) Li, Y.; Li, S.; Nagarajan, A. V.; Liu, Z.; Nevins, S.; Song, Y.; Mpourmpakis, G.; Jin, R. Hydrogen Evolution Electrocatalyst Design: Turning Inert Gold into Active Catalyst by Atomically Precise Nanochemistry. *J. Am. Chem. Soc.* **2021**, *143* (29), 11102−11108.
(106) Alfonso, D. R.; Kauffman, D.; Matranga, C. Active Sites of Ligand-Protected Au_{25} Nanoparticle Catalysts for CO_2 Electroreduction to CO. *J. Chem. Phys.* **2016**, *144* (18), 184705.
(107) Shen, H.; Wu, Q.; Malola, S.; Han, Y.-Z.; Xu, Z.; Qin, R.; Tang, X.; Chen, Y.-B.; Teo, B. K.; Häkkinen, H.; Zheng, N. N-Heterocyclic Carbene-Stabilized Gold Nanoclusters with Organometallic Motifs for Promoting Catalysis. *J. Am. Chem. Soc.* **2022**, *144* (24), 10844−10853.
(108) Chai, J.; Chong, H.; Wang, S.; Yang, S.; Wu, M.; Zhu, M. Controlling the Selectivity of Catalytic Oxidation of Styrene over Nanocluster Catalysts. *RSC Adv.* **2016**, *6* (112), 111399−111405.
(109) Austin, N.; Zhao, S.; McKone, J. R.; Jin, R.; Mpourmpakis, G. Elucidating the Active Sites for CO_2 Electroreduction on Ligand-Protected Au_{25} Nanoclusters. *Catal. Sci. Technol.* **2018**, *8* (15), 3795−3805.
(110) Seong, H.; Efremov, V.; Park, G.; Kim, H.; Yoo, J. S.; Lee, D. Atomically Precise Gold Nanoclusters as Model Catalysts for Identifying Active Sites for Electroreduction of CO_2. *Angew. Chem., Int. Ed.* **2021**, *60* (26), 14563−14570.
(111) Nonappa; Lahtinen, T.; Haataja, J. S.; Tero, T.-R.; Häkkinen, H.; Ikkala, O. Template-Free Supracolloidal Self-Assembly of Atomically Precise Gold Nanoclusters: From 2D Colloidal Crystals to Spherical Capsids. *Angew. Chem., Int. Ed.* **2016**, *55* (52), 16035−16038.
(112) Hossain, S.; Imai, Y.; Motohashi, Y.; Chen, Z.; Suzuki, D.; Suzuki, T.; Kataoka, Y.; Hirata, M.; Ono, T.; Kurashige, W.; Kawawaki, T.; Yamamoto, T.; Negishi, Y. Understanding and Designing One-Dimensional Assemblies of Ligand-Protected Metal Nanoclusters. *Mater. Horiz.* **2020**, *7* (3), 796−803.
(113) Yuan, P.; Zhang, R.; Selenius, E.; Ruan, P.; Yao, Y.; Zhou, Y.; Malola, S.; Häkkinen, H.; Teo, B. K.; Cao, Y.; Zheng, N. Solvent-Mediated Assembly of Atom-Precise Gold−Silver Nanoclusters to Semiconducting One-Dimensional Materials. *Nat. Commun.* **2020**, *11* (1), 2229.
(114) Liu, X.; Saranya, G.; Huang, X.; Cheng, X.; Wang, R.; Chen, M.; Zhang, C.; Li, T.; Zhu, Y. $Ag_2Au_{50}(PET)_{36}$ Nanocluster: Dimeric Assembly of $Au_{25}(PET)_{18}$ Enabled by Silver Atoms. *Angew. Chem., Int. Ed.* **2020**, *59* (33), 13941−13946.
(115) Song, Y.; Li, Y.; Li, H.; Ke, F.; Xiang, J.; Zhou, C.; Li, P.; Zhu, M.; Jin, R. Atomically Resolved $Au_{52}Cu_{72}(SR)_{55}$ Nanoalloy Reveals Marks Decahedron Truncation and Penrose Tiling Surface. *Nat. Commun.* **2020**, *11* (1), 478.
(116) Higaki, T.; Liu, C.; Zhou, M.; Luo, T.-Y.; Rosi, N. L.; Jin, R. Tailoring the Structure of 58-Electron Gold Nanoclusters: $Au_{103}S_2(S\text{-}Nap)_{41}$ and Its Implications. *J. Am. Chem. Soc.* **2017**, *139* (29), 9994−10001.
(117) De Nardi, M.; Antonello, S.; Jiang, D.; Pan, F.; Rissanen, K.; Ruzzi, M.; Venzo, A.; Zoleo, A.; Maran, F. Gold Nanowired: A Linear $(Au_{25})n$ Polymer from Au_{25} Molecular Clusters. *ACS Nano* **2014**, *8* (8), 8505−8512.
(118) Wu, Z.; Dong, C.; Li, Y.; Hao, H.; Zhang, H.; Lu, Z.; Yang, B. Self-Assembly of Au_{15} into Single-Cluster-Thick Sheets at the Interface of Two Miscible High-Boiling Solvents. *Angew. Chem., Int. Ed.* **2013**, *52* (38), 9952−9955.
(119) Wu, Z.; Liu, J.; Li, Y.; Cheng, Z.; Li, T.; Zhang, H.; Lu, Z.; Yang, B. Self-Assembly of Nanoclusters into Mono-, Few-, and Multilayered Sheets via Dipole-Induced Asymmetric van Der Waals Attraction. *ACS Nano* **2015**, *9* (6), 6315−6323.
(120) Li, Y.; Zhou, M.; Song, Y.; Higaki, T.; Wang, H.; Jin, R. Double-Helical Assembly of Heterodimeric Nanoclusters into Supercrystals. *Nature* **2021**, *594* (7863), 380−384.
(121) Shen, H.; Xu, Z.; Wang, L.; Han, Y.-Z.; Liu, X.; Malola, S.; Teo, B. K.; Häkkinen, H.; Zheng, N. Tertiary Chiral Nanostructures from C−H···F Directed Assembly of Chiroptical Superatoms. *Angew. Chem., Int. Ed.* **2021**, *60* (41), 22411−22416.
(122) Li, H.; Wang, P.; Zhu, C.; Zhang, W.; Zhou, M.; Zhang, S.; Zhang, C.; Yun, Y.; Kang, X.; Pei, Y.; Zhu, M. Triple-Helical Self-Assembly of Atomically Precise Nanoclusters. *J. Am. Chem. Soc.* **2022**, *144* (50), 23205−23213.
(123) Wu, Z.; Gayathri, C.; Gil, R. R.; Jin, R. Probing the Structure and Charge State of Glutathione-Capped $Au_{25}(SG)_{18}$ Clusters by NMR and Mass Spectrometry. *J. Am. Chem. Soc.* **2009**, *131* (18), 6535−6542.
(124) Yao, Q.; Yuan, X.; Yu, Y.; Yu, Y.; Xie, J.; Lee, J. Y. Introducing Amphiphilicity to Noble Metal Nanoclusters via Phase-Transfer Driven Ion-Pairing Reaction. *J. Am. Chem. Soc.* **2015**, *137* (5), 2128−2136.
(125) Sánchez, S.; Soler, L.; Katuri, J. Chemically Powered Micro- and Nanomotors. *Angew. Chem., Int. Ed.* **2015**, *54* (5), 1414−1444.
(126) Yao, Y.; Chen, Y.; Wang, H.; Samorì, P. Organic Photodetectors Based on Supramolecular Nanostructures. *SmartMat* **2020**, *1* (1). DOI: 10.1002/smm2.1009.
(127) Zhang, Z.; Yu, Y.; Yu, H.; Feng, Y.; Feng, W. Water-Resistant Conductive Organogels with Sensation and Actuation Functions for Artificial Neuro-Sensory Muscular Systems. *SmartMat* **2022**, *3* (4), 632−643.
(128) Chen, C.; Ding, S.; Wang, J. Materials Consideration for the Design, Fabrication and Operation of Microscale Robots. *Nat. Rev. Mater.* **2024**, *9* (3), 159−172.
(129) Luo, Y.; Wu, D.; Li, Z.; Li, X.-Y.; Wu, Y.; Feng, S.-P.; Menon, C.; Chen, H.; Chu, P. K. Plasma Functionalized MoSe2 for Efficient Nonenzymatic Sensing of Hydrogen Peroxide in Ultra-Wide pH Range. *SmartMat* **2022**, *3* (3), 491−502.
(130) Meng, X.; Qiu, L.; Xi, G.; Wang, X.; Guo, L. Smart Design of High-Performance Surface-Enhanced Raman Scattering Substrates. *SmartMat* **2021**, *2* (4), 466−487.
(131) Zanetti-Polzi, L.; Charchar, P.; Yarovsky, I.; Corni, S. Origins of the PH-Responsive Photoluminescence of Peptide-Functionalized Au Nanoclusters. *ACS Nano* **2022**, *16* (12), 20129−20140.
(132) Xie, J.; Zheng, Y.; Ying, J. Y. Highly Selective and Ultrasensitive Detection of Hg^{2+} Based on Fluorescence Quenching of Au Nanoclusters by Hg^{2+}−Au^{+} Interactions. *Chem. Commun.* **2010**, *46* (6), 961−963.
(133) Zhang, L.; Wang, E. Metal Nanoclusters: New Fluorescent Probes for Sensors and Bioimaging. *Nano Today* **2014**, *9* (1), 132−157.
(134) Qian, S.; Wang, Z.; Zuo, Z.; Wang, X.; Wang, Q.; Yuan, X. Engineering Luminescent Metal Nanoclusters for Sensing Applications. *Coord. Chem. Rev.* **2022**, *451*, No. 214268.